

# MR Pulse Sequences: What Every Radiologist Wants to Know but Is Afraid to Ask<sup>1</sup>

## TEACHING POINTS

See last page

*Richard Bitar, MD, MSc • General Leung, MSc • Richard Perng, MD  
Sameh Tadros, MD • Alan R. Moody, FRCR, FRCP • Josee Sarrazin,  
MD, FRCP • Caitlin McGregor, MD, FRCP • Monique Christakis, MD,  
FRCP • Sean Symons, MD, FRCP • Andrew Nelson, RTR, RTMR  
Timothy P. Roberts, PhD*

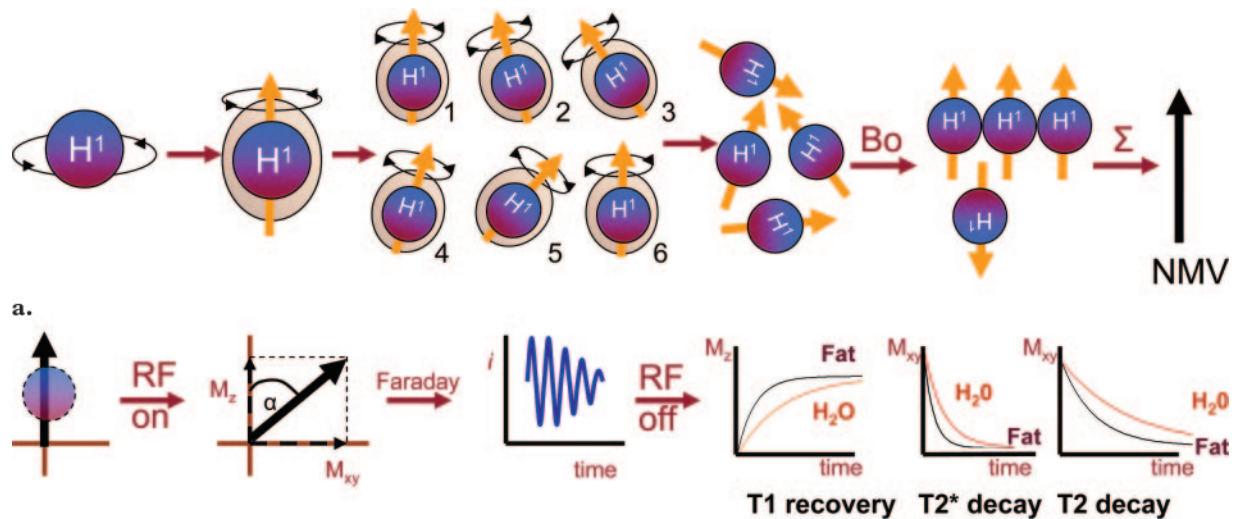
The use of magnetic resonance (MR) imaging is growing exponentially, in part because of the excellent anatomic and pathologic detail provided by the modality and because of recent technologic advances that have led to faster acquisition times. Radiology residents now are introduced in their 1st year of training to the MR pulse sequences routinely used in clinical imaging, including various spin-echo, gradient-echo, inversion-recovery, echo-planar imaging, and MR angiographic sequences. However, to make optimal use of these techniques, radiologists also need a basic knowledge of the physics of MR imaging, including T1 recovery, T2 and T2\* decay, repetition time, echo time, and chemical shift effects. In addition, an understanding of contrast weighting is very helpful to obtain better depiction of specific tissues for the diagnosis of various pathologic processes.

©RSNA, 2006

**Abbreviations:** ADC = apparent diffusion coefficient, FLAIR = fluid-attenuated inversion recovery, GRE = gradient echo, MOTSA = multiple overlapping thin-slab acquisitions, RF = radiofrequency, SAR = specific absorption rate, SE = spin echo, SSFP = steady-state free precession, STIR = short inversion time inversion recovery, TE = echo time, 3D = three-dimensional, TI = inversion time, TR = repetition time, 2D = two-dimensional

RadioGraphics 2006; 26:513-537 • Published online 10.1148/rg.262055063 • Content Codes: **MR** **PH**

<sup>1</sup>From the Department of Medical Imaging, University of Toronto, Fitzgerald Building, 150 College St, Room 112, Toronto, Ontario, Canada M5S 3E2 (R.B., A.R.M., J.S., C.M., M.C., S.S., T.P.R.); and Department of Medical Imaging, Sunnybrook and Women's College Health Sciences Centre, Toronto, Ontario, Canada (R.B., G.L., R.P., S.T., A.R.M., J.S., C.M., M.C., S.S., A.N.). Recipient of an Excellence in Design award for an education exhibit at the 2004 RSNA Annual Meeting. Received March 24, 2005; revision requested May 12 and received June 7; accepted July 6. All authors have no financial relationships to disclose. Address correspondence to R.B. (e-mail: [richard.bitar@utoronto.ca](mailto:richard.bitar@utoronto.ca)).



a.

**Figure 1.** Basic physics of the MR signal. **(a)** As  $^1\text{H}$  nuclei spin, they induce their own magnetic field (tan), the direction (magnetic axis) of which is depicted by an arrow (yellow). The  $^1\text{H}$  nuclei initially precess with a wobble at various angles (1–6), but when they are exposed to an external magnetic field ( $B_0$ ), they align with it. The sum of all magnetic moments is called the net magnetization vector (NMV). **(b)** When an RF pulse is applied, the net magnetization vector is flipped at an angle ( $\alpha$ ), which produces two magnetization components: longitudinal magnetization ( $M_z$ ) and transverse magnetization ( $M_{xy}$ ). As the transverse magnetization precesses around a receiver coil, it induces a current ( $i$ ). When the RF generator is turned off, T1 recovery and T2 and T2\* decay occur.

## Introduction

Not long ago, many radiology residents did not study magnetic resonance (MR) imaging until their senior year; however, with recent technological advances, including faster acquisition times and better anatomic and pathologic depiction, MR imaging is used with increasing frequency. In fact, residents now receive training in MR imaging and routinely use it while on call as early as the 1st year of residency. However, when residents are presented with MR images to interpret, they may not know where to start or, more important, why a specific pulse sequence with a particular contrast weighting was used. They may know little or nothing about the physical principles on which the sequence is based.

In this article, we describe the physical basis of the most common MR pulse sequences routinely used in clinical imaging. This is a vast and complicated subject, and only the fundamentals could be presented here; however, many excellent general (1–4) and detailed (5–30) references about the subject are available. To enhance understanding, our explanation of the physical principles is simplified; to highlight their practical relevance, clinical examples are interspersed throughout the article.

## Physics Overview

MR imaging is based on the electromagnetic activity of atomic nuclei. Nuclei are made up of protons and neutrons, both of which have spins. MR-active nuclei are those that have a net spin because they are odd-numbered and the spins of their protons and neutrons do not cancel each other out (5). In clinical MR imaging, hydrogen ( $^1\text{H}$ ) nuclei are used most often because of their abundance in the body, but other nuclei—for example, fluorine ( $^{19}\text{F}$ ) nuclei—also may be used (6).

Each nucleus rotates around its own axis. As the nucleus spins, its motion induces a magnetic field (Fig 1a). When the nuclei are exposed to an external magnetic field ( $B_0$ ), the interaction of the magnetic fields (ie, the fields of the spinning nuclei and the externally applied field) causes the nuclei to wobble, or precess. The frequency at which precession occurs is defined by the Larmor equation,  $\omega_0 = B_0 \times \gamma$ , where  $\omega_0$  is the precessional frequency,  $B_0$  is the external magnetic field strength (measured in teslas), and  $\gamma$  is the gyromagnetic ratio (measured in megahertz per tesla), which is a constant for every atom at a particular magnetic field strength (eg, for  $^1\text{H}$ ,  $\gamma/2\pi = 42.57$  MHz/T) (7).

Until the  $^1\text{H}$  nuclei are exposed to  $B_0$  magnetization, their axes are randomly aligned. However,

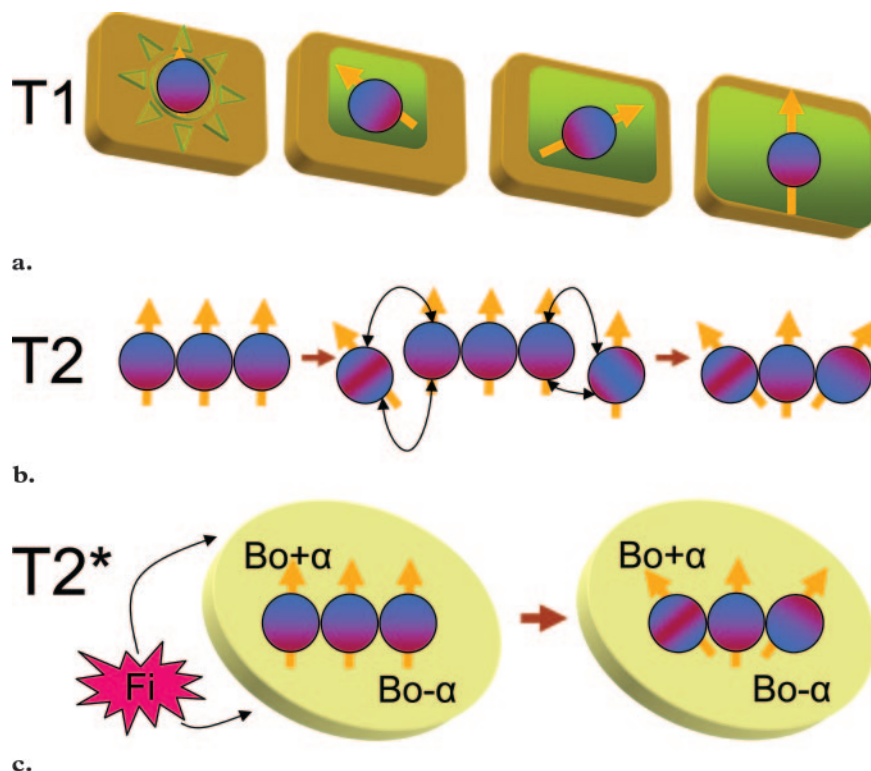


**Figure 2.** Magnetization relaxation and decay. **(a)** T1 recovery (spin-lattice relaxation) involves recovery of the longitudinal magnetization (yellow) because of the release of energy (green) into the environment. The lattice is indicated in tan. **(b)** T2 decay (spin-spin relaxation) is decay of the transverse magnetization because of the interaction of the individual magnetic fields of spinning nuclei. Note that all nuclei initially spin in phase (as indicated by the similar position of the red bands at the bottom of each circle), then move out of phase (with red bands in different positions). **(c)** T2\* decay is decay of the transverse magnetization because of magnetic field inhomogeneities ( $Fi$ ).  $\alpha$  = flip angle,  $B_0$  = external magnetic field.

when  $B_0$  magnetization is applied, the magnetic axes of the nuclei align with the magnetic axis of  $B_0$ , some in parallel and others in opposition to it (5) (Fig 1a). The cumulative effect of all the magnetic moments of the nuclei is the net magnetization vector. When a radiofrequency (RF) pulse is applied, the RF excitation causes the net magnetization vector to flip by a certain angle, and this produces two magnetization vector components, longitudinal magnetization and transverse magnetization (Fig 1b). As the transverse magnetization precesses around a receiver coil, it induces a current in that coil, in accordance with the Faraday law of induction (8). This current becomes the MR signal.

When the RF energy source is turned off, the net magnetization vector realigns with the axis of  $B_0$  through the process of T1 recovery, during which the longitudinal magnetization increases in magnitude, or recovers. At the same time, the transverse magnetization decreases (decays) through additional mechanisms known as T2\* decay and T2 decay. Different tissues have different T1, T2, and T2\* values. Furthermore, T2\* is dependent on the magnetic environment (the spatial uniformity of the external field). Fat has a shorter T1 (ie, recovers faster) and a shorter T2 (ie, decays faster) than water, which has a rela-

tively long T1 and T2. T2\* decay occurs very quickly in both fat and water (Fig 1b) (9).

During T1 (spin-lattice) relaxation, the longitudinal magnetization recovers as the spinning nuclei release energy into the environment (Fig 2a). During T2 (spin-spin) relaxation, the transverse magnetization is dephased because of interaction between the spinning nuclei and their magnetic fields (Fig 2b). In T2\* signal decay, the transverse magnetization is dephased because of magnetic field inhomogeneities. The magnetic field is not exactly the same everywhere; in some places it is a bit stronger ( $B_0 + \alpha$ )—for example, 1.505 T—and in others it is a bit weaker ( $B_0 - \alpha$ )—for example, 1.495 T. Such differences may occur because of the presence of metallic objects, air, dental implants, or calcium, or they may be due to the limitations of magnet construction (Fig 2c) (6).

As mentioned earlier, the transverse component of the net magnetization vector induces a current in the receiver coil. For the induction of current, the nuclei must be spinning in phase; as the nuclei gradually spin out of phase, the signal induced in the coil decreases. This process is

Teaching  
Point

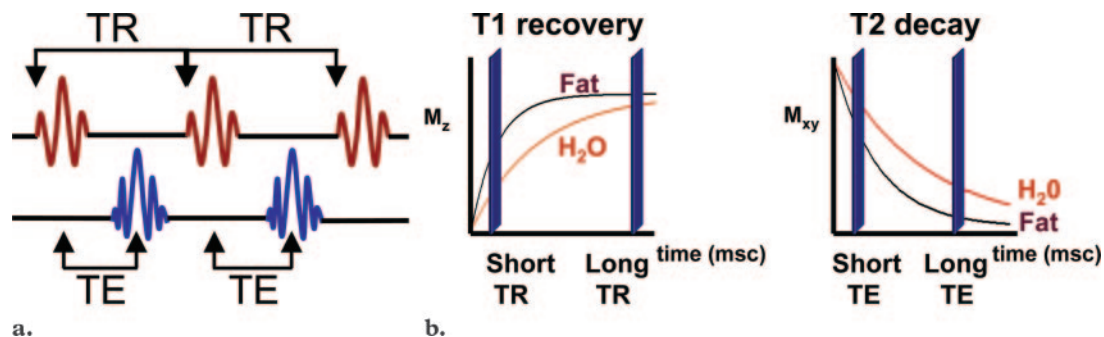


**Figure 4.** (a) Schematic representation of TR and TE. (b) Graphs show the effects of short and long TR (left) and short and long TE (right) on T1 recovery and T2 decay in fat and water: TR relates to T1 and affects T1 weighting, whereas TE relates to T2 and affects T2 weighting. *msc* = milliseconds,  $M_{xy}$  = transverse magnetization,  $M_z$  = longitudinal magnetization.

called free induction decay: *Free* refers to the fact that the system is no longer being forced out of equilibrium by the RF excitation; *induction* describes the mechanism through which the signal is detected; and *decay* refers to the decrease in signal amplitude over time.

### Repetition Time and Echo Time

At MR imaging, differences in T1, T2, and proton density (ie, the number of <sup>1</sup>H nuclei) in various tissues create differences in tissue contrast on images (9). Two key parameters—repetition time (TR) and echo time (TE)—are key to the creation of image contrast. Figure 3 shows the symbols that are most commonly used to diagram pulse sequences (1–3) as well as the echoes detected, including the Hahn echo (with use of a spin-echo [SE] pulse sequence) and the gradient echo (GRE) (10). It is important to recognize these symbols, because they are invariably used to represent TR and TE.

TR is the time (usually measured in milliseconds) between the application of an RF excitation pulse and the start of the next RF pulse (1,2). TE (also usually measured in milliseconds) is the time between the application of the RF pulse and the peak of the echo detected (Fig 4a) (1,2). Both parameters affect contrast on MR images because they provide varying levels of sensitivity to differences in relaxation time between various tissues. At short TRs, the difference in relaxation time between fat and water can be detected (longitudinal magnetization recovers more quickly in fat than in water); at long TRs, it cannot be detected. Therefore, TR relates to T1 (Fig 4b) and affects

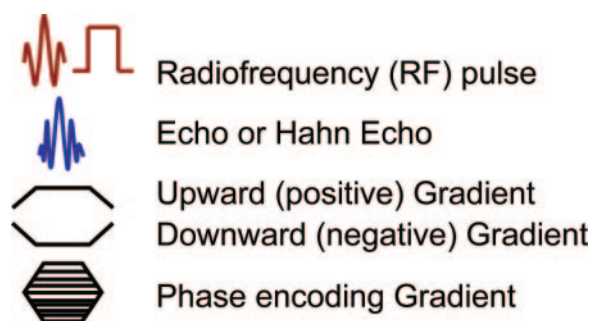


**Figure 3.** Definitions of common symbols used in pulse sequence diagrams.

contrast on T1-weighted images. At short TEs, differences in the T2 signal decay in fat and water cannot be detected; at long TEs, they can be detected. Therefore, TE relates to T2 (Fig 4b) and affects contrast on T2-weighted images.

When the TR is long and the TE is short, the differences in magnetization recovery and in signal decay between fat and water are not distinguishable (Fig 4b); therefore, the contrast observed on the resultant MR images is predominantly due to the difference in proton density between the two tissue types. Tissues with more protons have higher signal intensity, and those with fewer protons have lower signal intensity.

### Tissue Contrast

All MR images are to some degree affected by each of the parameters that determine tissue contrast (ie, T1, T2, and proton density), but the TR and TE can be adjusted to emphasize a particular type of contrast. This may be done, for example, with T1 weighting. In T1-weighted MR imaging, while the images show all types of contrast, T1 contrast is accentuated. Table 1 describes the pa-

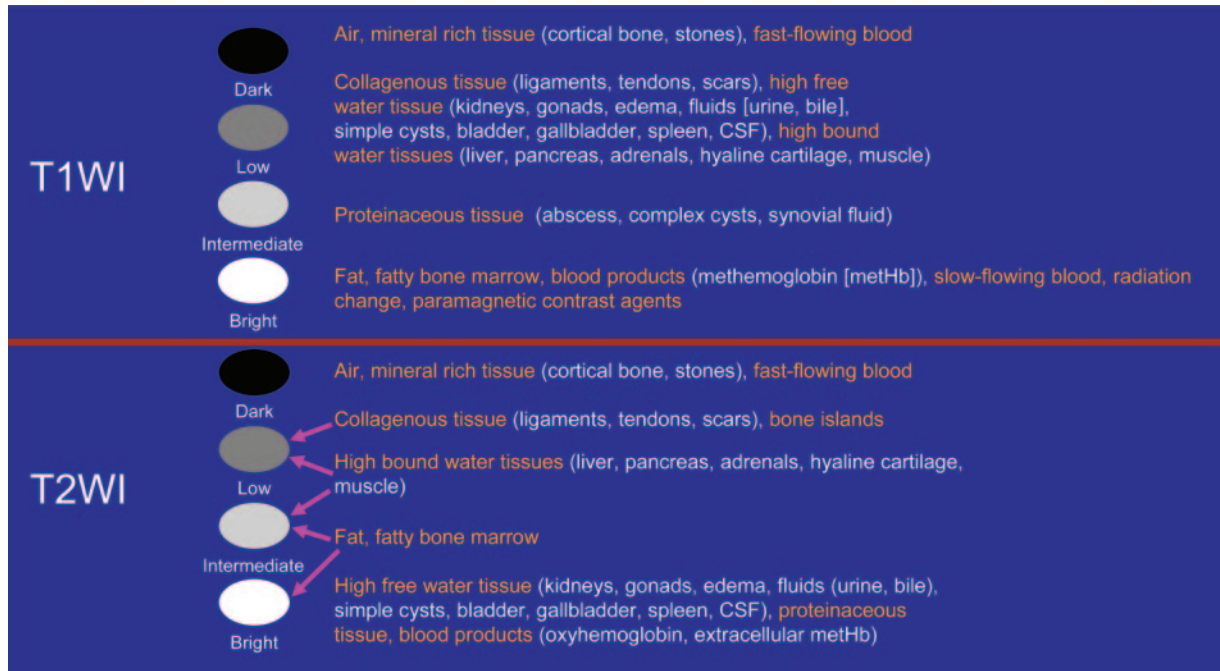


**Figure 5.** Diagram shows the signal intensity of various tissues at T1- and T2-weighted imaging. However, note that the signal characteristics of proteinaceous tissues vary according to the amount of protein content: Tissues with high concentrations of protein may have high signal intensity on T1-weighted images (*T1WI*) and low signal intensity on T2-weighted images (*T2WI*). *CSF* = cerebrospinal fluid. (Sources: References 1, 3, and 4.)

**Table 1**  
**Effect of TR and TE on MR Image Contrast**

| Imaging Technique        | TR    | TE    |
|--------------------------|-------|-------|
| T1 weighting             | Short | Short |
| T2 weighting             | Long  | Long  |
| Proton-density weighting | Long  | Short |

**Table 2**  
**Typical TR and TE Values for SE and GRE Sequences**

| Sequence | TR      |        | TE    |      |
|----------|---------|--------|-------|------|
|          | Short   | Long   | Short | Long |
| SE       | 250–700 | > 2000 | 10–25 | > 60 |
| GRE      | < 50    | > 100  | 1–5   | > 10 |

Note.—Values are given in milliseconds.

rameters used to obtain images with T1, T2, and proton-density weighting (1,3). T1-weighted images best depict the anatomy, and, if contrast material is used, they also may show pathologic entities; however, T2-weighted images provide the

best depiction of disease, because most tissues that are involved in a pathologic process have a higher water content than is normal, and the fluid causes the affected areas to appear bright on T2-weighted images (1,3,9). Proton-density weighted MR images usually depict both the anatomy and the disease entity. Table 2 shows typical TR and TE values that may be used to achieve different weighting with SE and GRE sequences (1,3). The levels of signal intensity that characterize various tissues on T1- and T2-weighted images are shown in Figure 5 (1,3,4).

**MR Signal Localization**

How does the MR imaging system detect which tissue the signal is coming from? For this purpose, gradients are employed. Gradients are linear variations of the magnetic field strength in a selected region (11). Along with the magnetic field strength, the precessional frequency of <sup>1</sup>H nuclei is also changed in the specific region (recall the Larmor equation). Three types of gradients are applied, according to the axis of imaging (x-, y-,

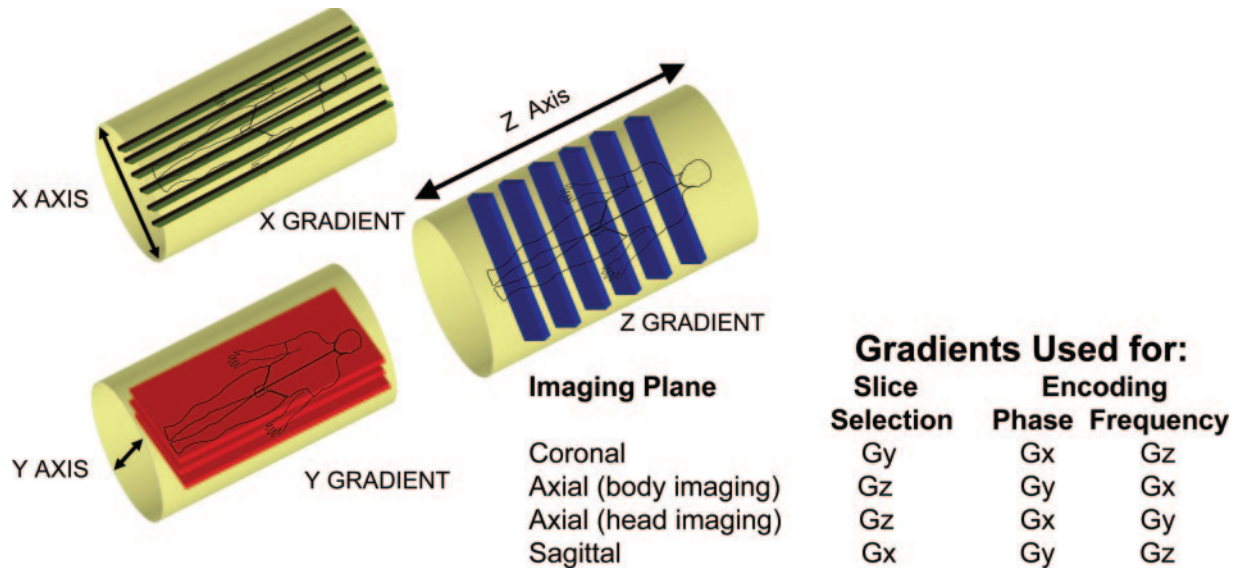


**Figure 6.** Schematic and table show the x-, y-, and z-axis gradients ( $G_x$ ,  $G_y$ , and  $G_z$ , respectively) that are used for section selection and for phase and frequency encoding during acquisitions in the most common imaging planes.

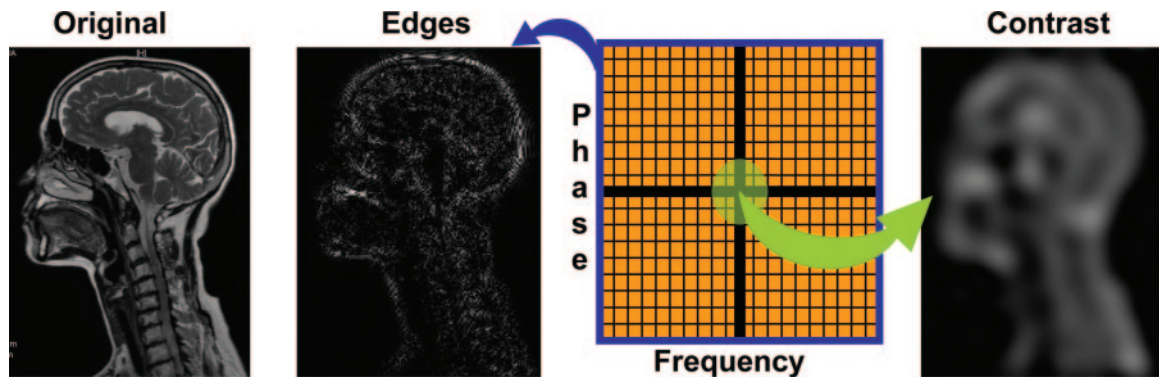


**Figure 7.** Schematic and corresponding MR images show the characteristics determined by data at the periphery of k-space (ie, spatial resolution, or definition of edges) and those determined by data at the center of k-space (ie, gross form and image contrast).

or z-axis) (Fig 6). The section-selective gradient selects the section to be imaged (ie, the target of the RF excitation pulse). The phase-encoding gradient causes a phase shift in the spinning protons so that the MR imaging system computer can detect and encode the phase of the spin (eg, the location of the red bands in the nuclei shown in Fig 2). The frequency-encoding gradient also causes a shift—one of frequency rather than phase—that helps the MR system to detect the location of the spinning nuclei. Because this shift

of frequency usually occurs when the echo is read, it is also called the readout gradient. Once the MR system processor has all of that information (ie, the frequency and phase of each spin), it can compute the exact location and amplitude of the signal. That information is then stored in k-space.

### k-Space and the Image Matrix

k-Space (named for  $k$ , the symbol for wave number) is a matrix of voxels within which the raw imaging data are stored in the MR imaging system (12). The horizontal axis (x-axis) of the matrix usually corresponds to the frequency, and the

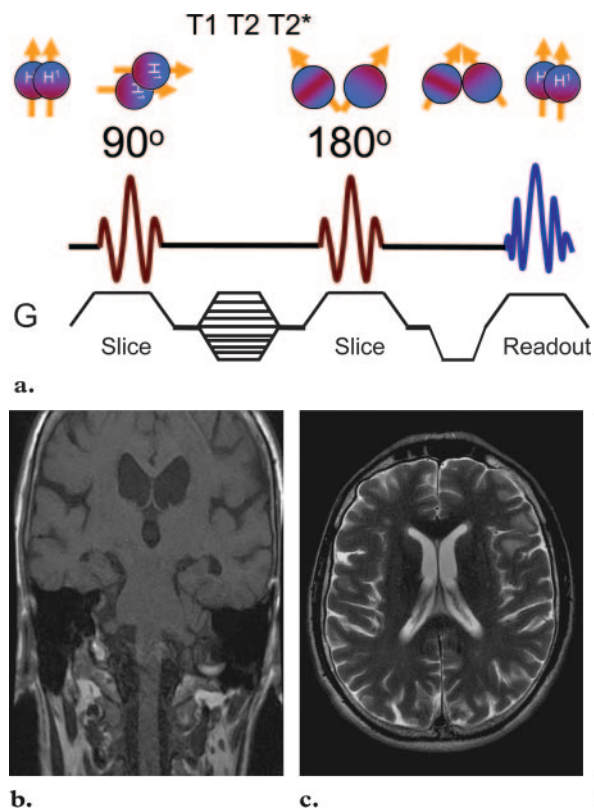


**Figure 8.** Application of an SE pulse sequence. (a) Diagram shows the application of an initial pulse at a 90° flip angle to redirect the net magnetization vector into the transverse plane; a subsequent interval of T1, T2, and T2\* relaxation, accompanied by the gradual dephasing of the transverse magnetization; and a second pulse applied at a flip angle of 180° to bring the spinning nuclei again into phase so that an echo is produced. Note the locations of the section-selective (*Slice*) and phase- and frequency-encoding (*Readout*) gradients (*G*). (b, c) Coronal T1-weighted (b) and axial T2-weighted (c) SE images of the brain. (d) Sagittal proton-density weighted SE image of the knee.

vertical axis (y-axis) usually corresponds to the phase (although the axes of frequency and phase may be easily interchanged) (Fig 7). The center of k-space contains information about gross form and tissue contrast, whereas the edges (periphery) of k-space contain information about spatial resolution (details and fine structures). The raw imaging data in k-space must be Fourier transformed to obtain the final image.

### Diagrams and Clinical Applications of MR Sequences

Pulse sequences are wave forms of the gradients and RF pulses applied in MR image acquisition (2). The diagrams may be composed of several parallel lines if each parameter is diagrammed separately, or they may consist of only one or two lines if the parameters are superimposed. If the parameters are diagrammed separately, at least four lines are required: one for the RF pulse, and one each for the x-, y-, and z-axis gradients (2). The pulse sequence diagram is a schema of the

timing of instructions sent to the RF generator and gradient amplifiers.

There are only two fundamental types of MR pulse sequences: SE and GRE. All other MR sequences are variations of these, with different parameters added on. MR pulse sequences can be either two-dimensional (2D), with one section acquired at a time, or three-dimensional (3D), with a volume of multiple sections obtained in a single acquisition.

### SE Sequences

In SE sequences, a 90° pulse flips the net magnetization vector into the transverse plane (10). As the spinning nuclei go through T1, T2, and T2\* relaxation, the transverse magnetization is gradually dephased. A 180° pulse is applied at a time equal to one-half of TE to rephase the spinning nuclei. When the nuclei are again spinning in phase (at total TE), an echo is produced and read (Fig 8a). Most conventional SE sequences are

Teaching Point

**Table 3**  
Common and Trade Names for SE Sequences Used by Major Vendors

| Pulse Sequence   | GE Healthcare  | Siemens Medical Solutions                                | Philips Medical Systems  |
|------------------|--|--|--------------------------|
| Single-echo SE   | SE   | Single SE  | SE, modified SE          |
| Multiple-echo SE | Multiecho multiplanar (MEMP), variable echo multiplanar (VEMP) | SE, double echo  | Multiple SE (MSE)        |
| Echo-train SE    | Fast SE (FSE), single-shot fast SE (SSFSE)                     | TurboSE (TSE), half-Fourier acquisition turbo SE (HASTE) | TSE, ultrafast SE (UFSE) |

Note.—Adapted, with permission, from reference 2.

**Figure 9.** MR cholangiopancreatography. Sagittal fast SE image obtained with a heavily T2-weighted sequence (TE = 650) shows the common hepatic duct (arrowhead) and common bile duct (arrow).



very long and therefore are not used frequently. However, advances in MR imaging technology have enabled a reduction in acquisition time with the use of fast SE sequences. Table 3 shows the names of the various SE sequences used by the major MR imaging system vendors.

As mentioned earlier, sequences that have a short TR and short TE are used to obtain T1 weighting. Those with a long TR and short TE result in proton-density weighting. When the TR is long and the TE is long, T2 weighting is achieved. Sequentially increasing the TE of a sequence weights it more heavily toward T2: This technique is used at MR cholangiopancreatography to obtain a detailed depiction of the bile ducts and pancreatic ducts (Fig 9). Increasing the TE also is

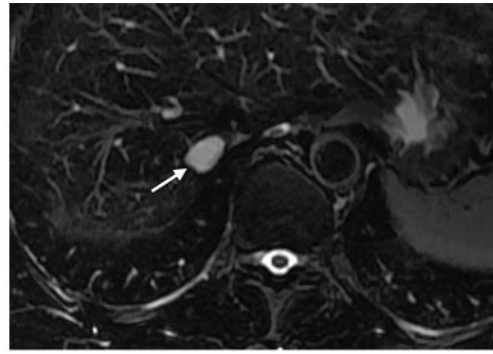
useful for MR imaging of hemangiomas and cysts (Fig 10). Clinical illustrations of the contrast weightings of tissues and the advantages of choosing a particular contrast weighting at SE or fast SE MR imaging are shown in Figures 8–11.

### SE-based Sequences

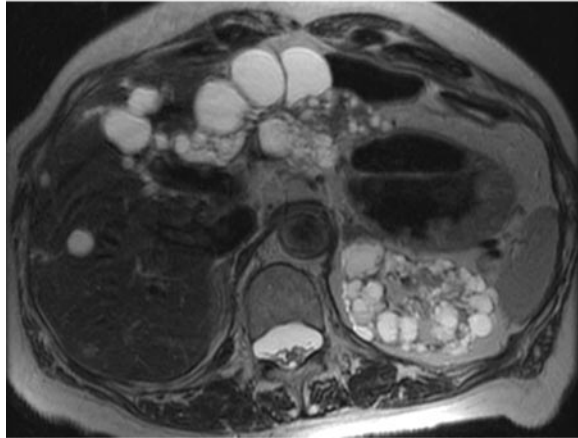
**Fast SE Variants.**—In a fast or turbo SE sequence, a single  $90^\circ$  pulse is applied to flip the net magnetization vector, after which multiple  $180^\circ$  rephasing pulses are applied (13), each of which



a.

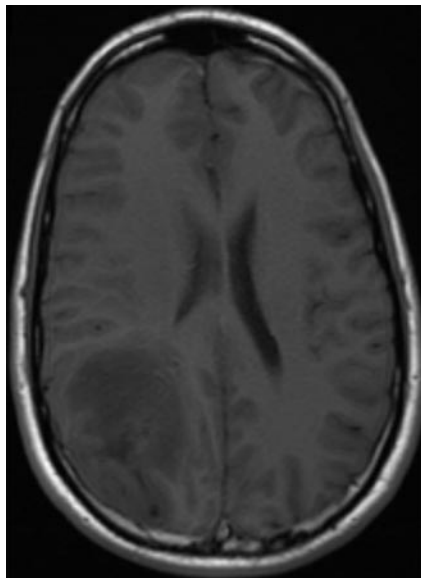


b.

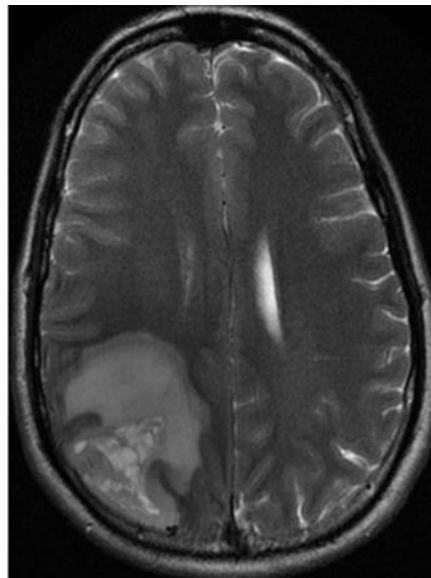


c.

**Figure 10.** Clinical examples of SE and fast SE sequences. **(a, b)** Liver hemangioma. **(a)** Axial T2-weighted fast SE image (TE = 82.9) shows a high-signal-intensity lesion (arrow) in the right lobe of the liver. **(b)** Axial T2-weighted fast SE image (TE = 180), obtained with heavier T2 weighting than **a**, shows retention of high signal intensity in the lesion (arrow), a feature that indicates a cyst or hemangioma. **(c)** Polycystic kidney disease. Axial T2-weighted fast SE image provides excellent depiction of cysts, which appear as areas of high signal intensity in the liver and kidney. Differences in signal intensity among the cysts are due to different protein concentrations.



a.



b.

**Figure 11.** Axial T1-weighted **(a)** and T2-weighted **(b)** fast SE images show a low-grade glioma. Because of hypercellularity, the tumor appears with hypointense signal in **a** and hyperintense signal in **b**. The cystic components and edema are better depicted in **b** than in **a**.

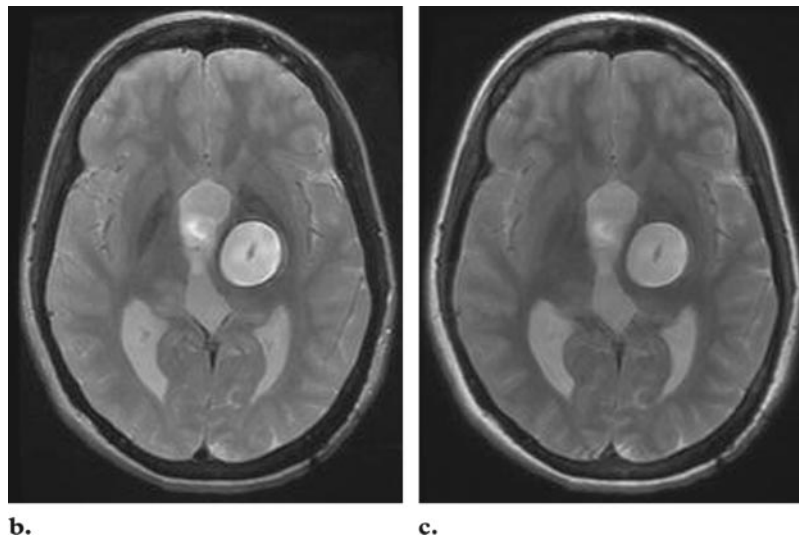
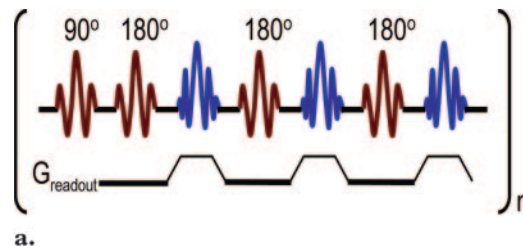


**Figure 12.** Fast SE pulse sequence. (a) Pulse sequence diagram shows the fast SE sequence used to obtain the image in b.  $G$  = gradient,  $n$  = number of repetitions. (b, c) Axial T2-weighted fast SE image (b) and conventional SE image (c) provide comparable depiction of a brain tumor. The acquisition time for conventional SE imaging was 7 minutes 17 seconds, whereas that for fast SE imaging with an echo train length of 16 was 34 seconds.

creates a Hahn echo (Fig 12a). All the echoes together are called an echo train, and the total number of  $180^\circ$  RF pulses and echoes is referred to as the echo train length. The acquisition time is greatly reduced with use of a fast SE sequence as opposed to a conventional SE sequence (Figs 12b, 12c). It is approximately proportional to  $1/ETL$ , where ETL is the echo train length, for imaging of a single section or a small number of sections. However, at imaging of larger volumes, the reduction of acquisition time is highly dependent on the spatial coverage.

**Conventional Inversion Recovery.**—This is an SE sequence in which a  $180^\circ$  preparatory pulse is applied to flip the net magnetization vector  $180^\circ$  and null the signal from a particular entity (eg, water in tissue). When the RF pulse ceases, the spinning nuclei begin to relax. When the net mag-

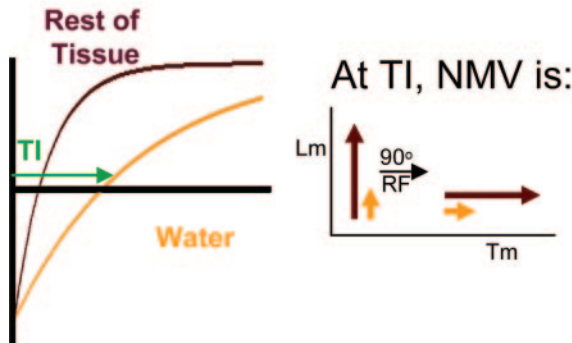
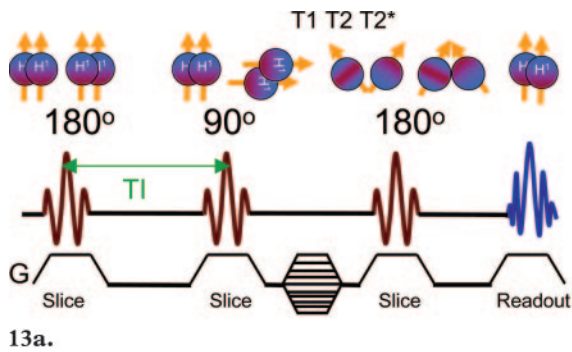
netization vector for water passes the transverse plane (the null point for that tissue), the conventional  $90^\circ$  pulse is applied, and the SE sequence then continues as before (Fig 13). The interval between the  $180^\circ$  pulse and the  $90^\circ$  pulse is the TI.

At TI, the net magnetization vector of water is very weak, whereas that for body tissues is strong (Fig 14). When the net magnetization vectors are flipped by the  $90^\circ$  pulse, there is little or no transverse magnetization in water, so no signal is generated (fluid appears dark), whereas signal intensity ranges from low to high in tissues with a stronger net magnetization vector. Two important clinical implementations of the inversion-recovery concept are the short TI inversion-recovery (STIR) sequence and the fluid-attenuated inversion-recovery (FLAIR) sequence. Table 4 shows the names of the various inversion-recovery sequences used by the major MR imaging system vendors.

**Table 4**  
**Common and Trade Names for Inversion-Recovery Sequences Used by Major Vendors**

| Pulse Sequence                | GE Healthcare                               | Siemens Medical Solutions | Philips Medical Systems                        |
|-------------------------------|---|---------------------------|--|
| Standard inversion recovery   | Multiplanar inversion recovery (MPIR)       | Inversion recovery (IR)   | IR   |
| Echo-train inversion recovery | Fast multiplanar inversion recovery (FMPIR) | TurboIR                   | IR-turboSE                                     |
| Short T1 inversion recovery   | STIR  | STIR                      | Spectrally selective inversion recovery (SPIR) |

Note.—Adapted, with permission, from reference 2. STIR = short inversion time inversion recovery.



**Figures 13, 14.** (13a) Conventional inversion-recovery sequence diagram shows a 180° preparatory inversion pulse applied to null the signal from either fat or water. At a predetermined inversion time (TI), a 90° pulse is applied, and the SE sequence is continued. *G* = gradient. (13b) Coronal STIR image shows an insufficiency fracture of the distal tibia, with an extensive area of high signal intensity in bone marrow near the site of the fracture (arrow). (14) Diagrams show T1 recovery in water and in tissue with use of a conventional inversion-recovery sequence. Nulling of the water signal is seen at TI, when there is virtually no net magnetization vector (*NMV*) in water. When the 90° pulse flips the net magnetization vector into the transverse plane, little or no transverse magnetization (*Tm*) is present, and, therefore, no signal is detected in water. *Lm* = longitudinal magnetization.

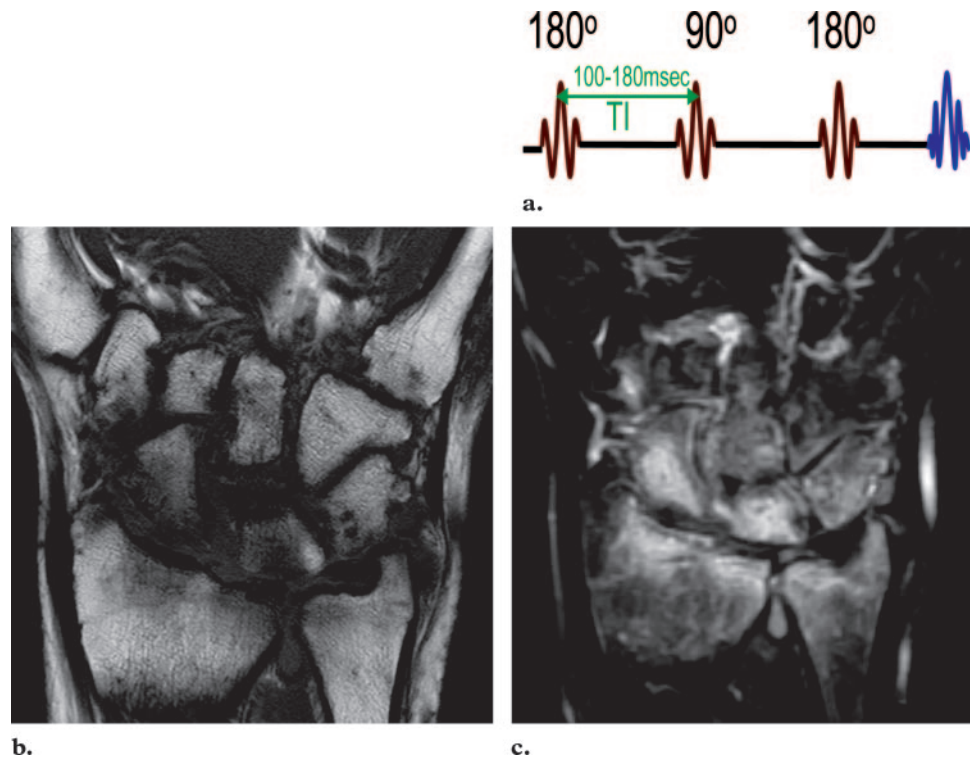


**Figure 15.** Comparison of fast SE and STIR sequences for depiction of bone marrow edema. **(a)** Diagram of the STIR sequence (TI = 100–180 msec for fat). **(b, c)** Coronal T1-weighted fast SE image **(b)** and coronal STIR image **(c)** both show pancarpal rheumatoid arthritis; however, the extent of bone marrow edema throughout the carpal bones, distal radius, and ulna is better depicted in **c** than in **b**.

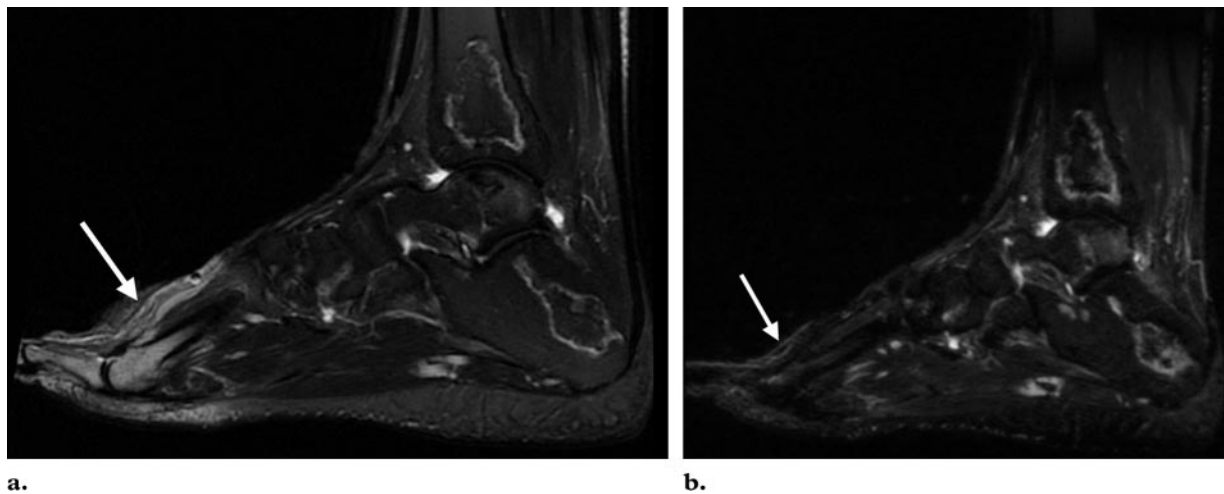
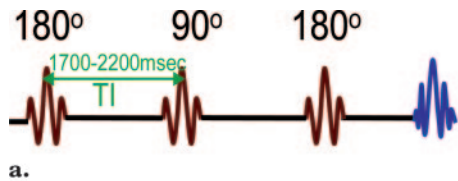
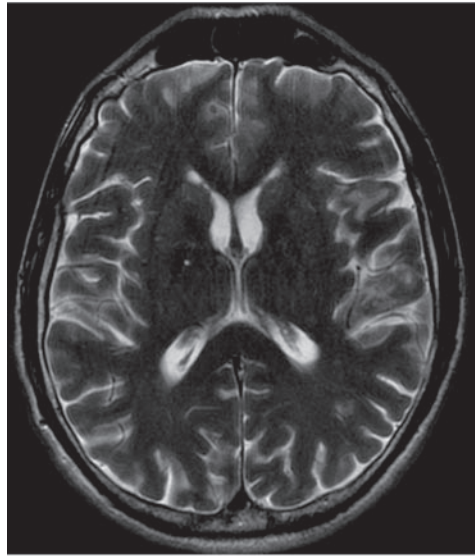


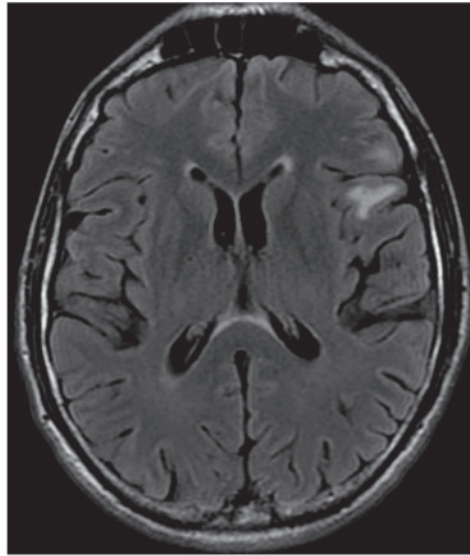
**Figure 16.** Comparison of magnetic field inhomogeneities with fast SE versus STIR sequences. **(a)** Sagittal T2-weighted fast SE image obtained with spectral fat suppression, which requires a uniform magnetic field, shows incomplete fat saturation in regions where there is field inhomogeneity, such as at the irregular air–soft tissue interfaces of the toes (arrow). **(b)** Sagittal image obtained with STIR, which is less susceptible than fast SE sequences to magnetic field inhomogeneities, provides more uniform and more complete fat saturation (arrow). Bone infarcts in the distal tibia and heel appear as areas of high signal intensity on both images.



a.



b.



c.

**Figure 17.** Comparison of fast SE and FLAIR sequences for depiction of lung cancer metastases to brain. (a) Diagram of the FLAIR sequence shows a TI of 1700–2200 msec for cerebrospinal fluid. (b) Axial T2-weighted fast SE image shows white matter abnormalities in the left temporal lobe. (c) Axial T2-weighted FLAIR image obtained with nulling of the signal from cerebrospinal fluid shows the metastatic lesions more clearly.

**STIR.**—In STIR sequences, an inversion-recovery pulse is used to null the signal from fat (14). When the net magnetization vector of fat passes its null point (at approximately 140 msec), the conventional  $90^\circ$  RF pulse is applied. Little or no longitudinal magnetization is present in fat, and the transverse magnetization in fat is insignificant. It is transverse magnetization that induces an electric current in the receiver coil, and, because the insignificant transverse magnetization of fat produces an insignificant current, no signal is generated from fat. STIR sequences provide excellent depiction of bone marrow edema (Fig 15), which may be the only indication of an occult fracture. Unlike conventional fat-saturation sequences (discussed later), STIR sequences are not affected by magnetic field inhomogeneities, so they are more efficient for nulling the signal from fat (Fig 16).

**FLAIR.**—In FLAIR sequences, an inversion-recovery pulse is used to null the signal from cere-

brospinal fluid (15). When the net magnetization vector of cerebrospinal fluid passes its null point, little or no longitudinal magnetization is present in the fluid. The transverse magnetization of cerebrospinal fluid is insignificant, and therefore no signal is generated (Fig 17). Elimination of the signal from cerebrospinal fluid is useful for detecting lesions that otherwise are not easily distinguishable or for delineating hyperintense lesions that border fluid-containing spaces such as sulci or ventricles in the brain (Fig 17b, 17c).

### GRE Sequences

In a GRE sequence, an RF pulse is applied that partly flips the net magnetization vector into the transverse plane (variable flip angle) (16). Gradients, as opposed to RF pulses, are used to dephase (negative gradient) and rephase (positive

**Table 5**  
**Comparison of SE and GRE Sequences**

| Criterion                                     | SE                                 | GRE                                |
|---|------------------------------------|------------------------------------|
| Rephasing mechanism                           | RF pulse                           | Variation of gradients             |
| Flip angle                                    | 90° only                           | Variable                           |
| Efficiency at reducing magnetic inhomogeneity | Very efficient (true T2 weighting) | Not very efficient (T2* weighting) |
| Acquisition time                              | Long (slow sequences)              | Short (fast sequences)             |

Note.—Adapted, with permission, from reference 3.

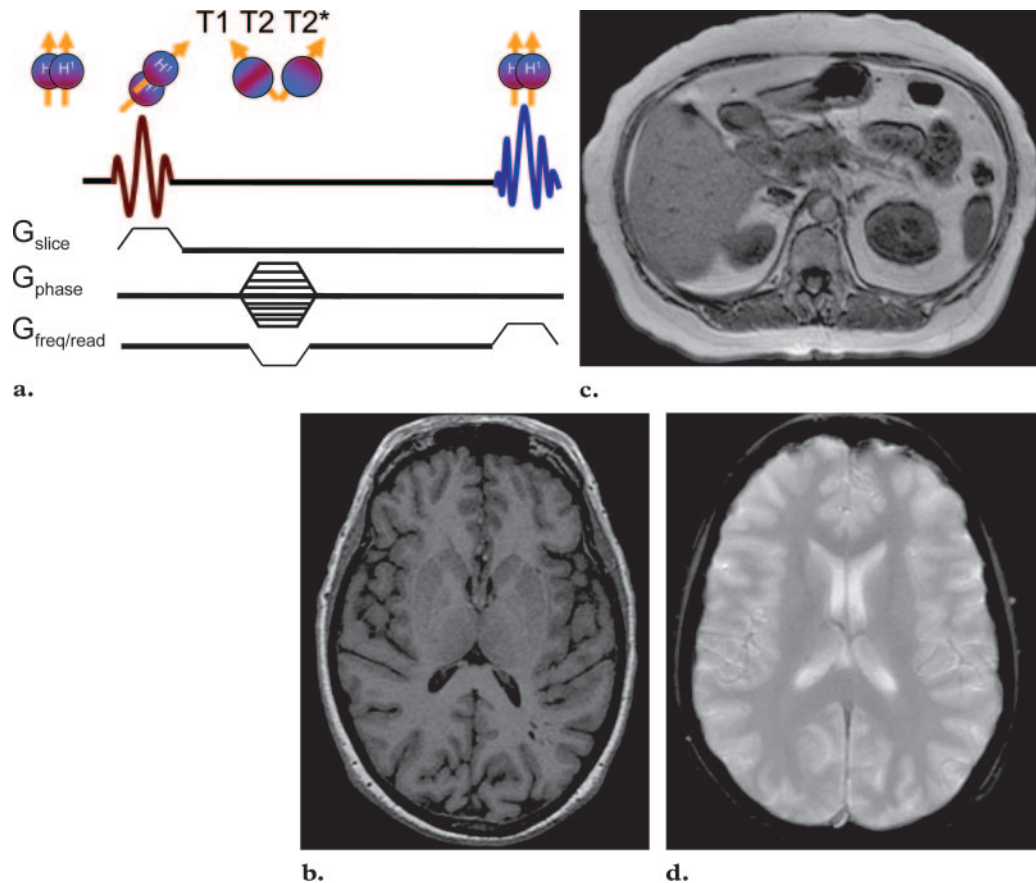


**Figure 18.** Comparison of T1-weighted and T2-weighted GRE pulse sequences. (a) GRE pulse sequence diagram shows a variable flip angle and the gradients used to dephase (negative) and rephase (positive) transverse magnetization. Note the locations of the section-selective ( $G_{slice}$ ), phase-encoding ( $G_{phase}$ ), and frequency-encoding ( $G_{freq/read}$ ) gradients. (b–d) Axial T1-weighted GRE images of the brain (b) and upper abdomen (c), and axial T2\*-weighted GRE image of the brain (d), obtained with the pulse sequence in a.

gradients) transverse magnetization (Figs 3, 18). Because gradients do not refocus field inhomogeneities, GRE sequences with long TEs are T2\* weighted (because of magnetic susceptibility) rather than T2 weighted like SE sequences. Table 5 lists important differences between SE and

GRE sequences. The names of various GRE sequences used by the major MR imaging system vendors are listed in Table 6.

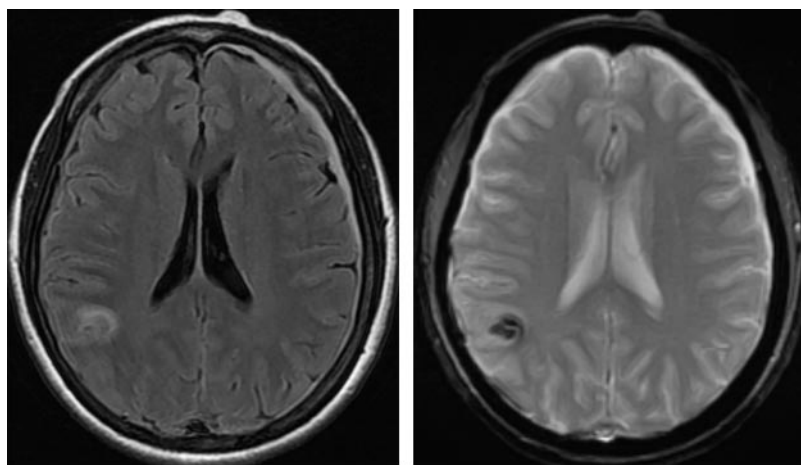
GRE sequences are sensitive to magnetic field inhomogeneity secondary to magnetic susceptibility differences between tissues. Magnetic susceptibility-related signal loss, or susceptibility artifact, is caused by magnetic field ( $B_0$ ) inhomoge-

Teaching  
Point

**Table 6**  
**Common Names for GRE Sequences Used by Major Vendors**

| Pulse Sequence             | GE Healthcare   | Siemens Medical Solutions  | Philips Medical Systems                       |
|----------------------------|---|--|---|
| Refocused, post-excitation | Gradient-recalled acquisition in the steady state (GRASS), fast GRASS, multiplanar GRASS (MPGR), fast multiplanar GRASS (FMPGR) | Fast imaging with steady-state precession (FISP)                             | Fast field echo (FFE)                         |
| Spoiled (incoherent)       | Spoiled GRASS (SPGR), fast spoiled GRASS (FSPGR), multiplanar spoiled GRASS (MPSPGR), fast multiplanar spoiled GRASS (FMPSPGR)  | Fast low-angle shot (FLASH)  | T1-weighted contrast-enhanced FFE (T1 CE-FFE) |
| Refocused, pre-excitation  | SSFP  | Reversed FISP (PSIF)   | T2-weighted contrast-enhanced FFE (T2 CE-FFE) |
| Magnetization prepared     | Inversion-recovery-prepared fast GRASS  | TurboFLASH, magnetization-prepared rapid acquisition gradient echo (MP-RAGE) | Turbo field echo (TFE)                        |

Note.—Adapted, with permission, from reference 2.



a.

b.

**Figure 19.** Comparison of FLAIR and GRE sequences for the depiction of hemorrhage. **(a)** Axial T2-weighted FLAIR image shows an area of high signal intensity in the right parietal lobe, a finding indicative of hemorrhage. **(b)** Axial T2-weighted GRE image shows signal loss due to the magnetic susceptibility of hemoglobin in the area of hemorrhage.

neity (17) and can be described in terms of T2\* signal decay. This inhomogeneity (local variation in  $B_0$ ) usually occurs at the interface between entities (eg, tissue and air) that have different magnetic susceptibilities. Because magnetic fields vary locally, some spinning nuclei precess faster (recall the Larmor equation,  $\omega_0 = B_0 \times \gamma$ ) than others; so when the individual vectors are added to obtain the net magnetization vector, there is a progressive decrease in the magnitude of the net magnetization vector over time. This decrease results in a progressive decrease in signal intensity, which eventually leads to a signal void. This feature of GRE sequences is exploited for the detection of hemorrhage, as the iron in hemoglobin becomes magnetized locally (produces its own

local magnetic field) and thus dephases the spinning nuclei. The technique is particularly helpful for diagnosing hemorrhagic contusions such as those in the brain (Fig 19) and in pigmented villonodular synovitis (Fig 20). SE sequences, on the other hand, while they are relatively immune from magnetic susceptibility artifacts, are also less sensitive in depicting hemorrhage and calcification.

Magnetic susceptibility imaging is the basis of cerebral perfusion studies, in which the T2\* effects (ie, signal decrease) created by gadolinium (a metal injected intravenously as a chelated ion in aqueous solution, typically in the form of

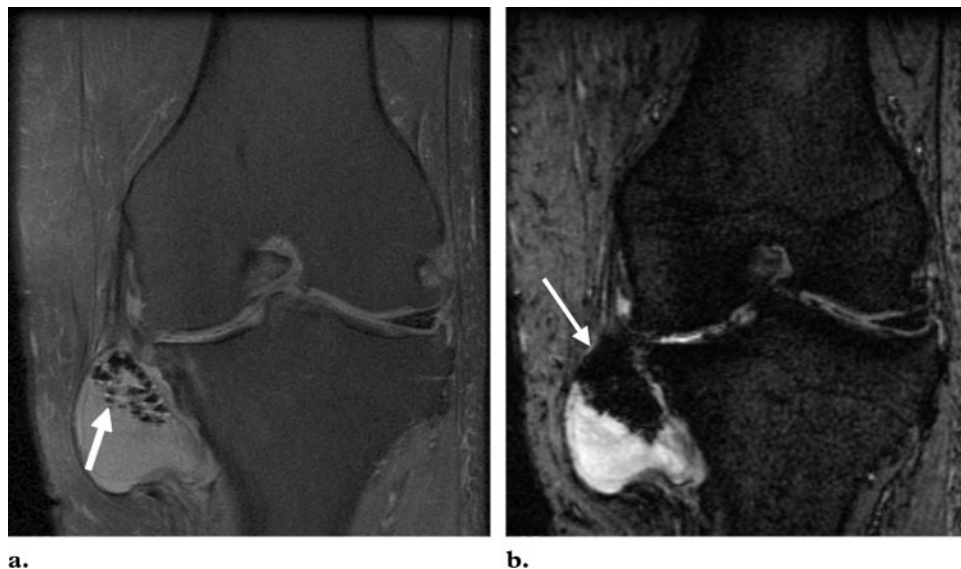


**Figure 20.** Pigmented villonodular synovitis. **(a)** Coronal proton-density weighted fast SE image obtained with fat saturation shows a large parameniscal cyst that contains punctate low-signal-intensity foci (arrow). **(b)** Coronal T2\*-weighted GRE image depicts the punctate foci (arrow) much more prominently, with a visual effect (blooming artifact) that is related to the magnetic susceptibility of hemosiderin in the area affected by pigmented villonodular synovitis.

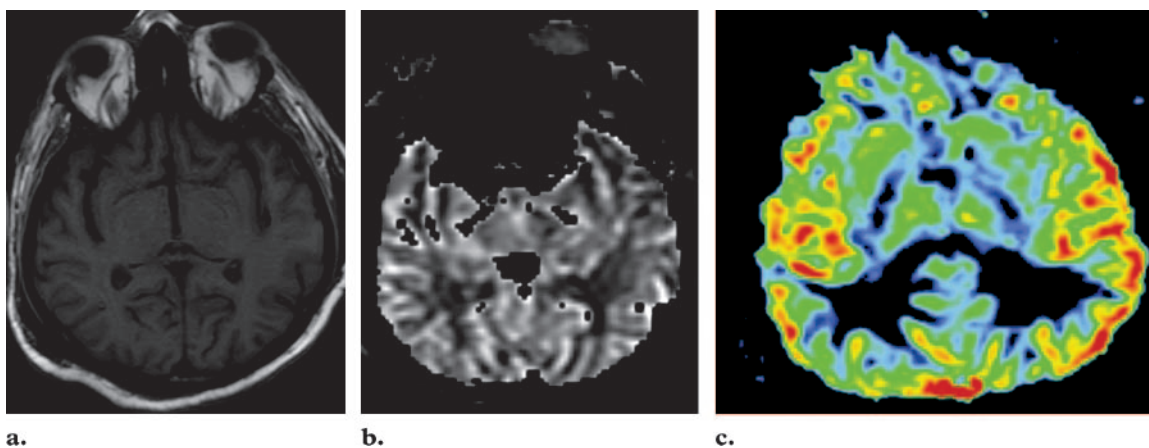


**Figure 21.** MR cerebral perfusion study with normal findings. **(a)** Axial T1-weighted SE image. **(b, c)** Corresponding perfusion images show negative enhancement **(b)** and the maximum enhancement slope **(c)**.

gadopentetate dimeglumine) are sensitively depicted by GRE sequences (18) (Fig 21). Magnetic susceptibility is also used in blood oxygenation level-dependent (BOLD) imaging, in which the relative amount of deoxyhemoglobin in the cerebral vasculature is measured as a reflection of neuronal activity. BOLD MR imaging is widely used for mapping of human brain function.

GRE sequences may be coherent (refocused) or incoherent (spoiled). Both sequence types usually involve the creation of a steady state (17). In the steady state, the TR is usually shorter than the T1 and T2 of the tissues imaged. Therefore, only

T2\* dephasing is allowed to occur. Because of this, the transverse magnetization does not have a chance to decay between successive TRs; that is, it remains in a steady state, essentially unmoving. Transverse magnetization therefore accumulates over time.

**Partially Refocused GRE.**—Coherent or partially refocused (rewound) GRE sequences use a gradient (called a rewind gradient) to rephase the T2\* magnetization while it is being dephased and thereby preserve the T2\* effects (20,21). Therefore, these sequences provide T2 weighting (Fig 22a). Partially refocused GRE sequences are especially useful for MR angiography and for depiction of the internal auditory canal (Fig 22a).

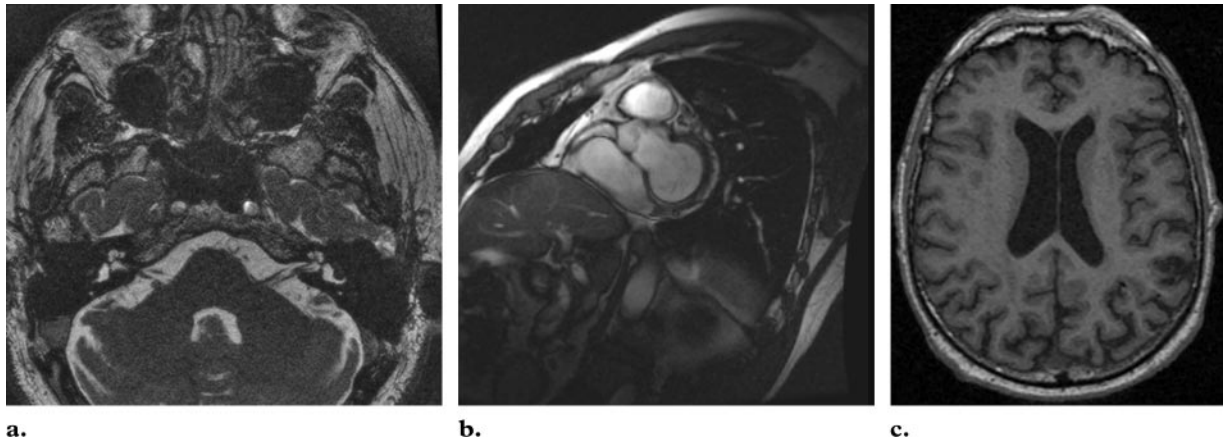


**Figure 22.** Spoiled and refocused GRE sequences. **(a)** Axial T2-weighted partially refocused (coherent) GRE image of the internal auditory canal. **(b)** Oblique sagittal T2-weighted SSFP image of the heart. **(c)** Axial T1-weighted spoiled (incoherent) GRE image of the brain.

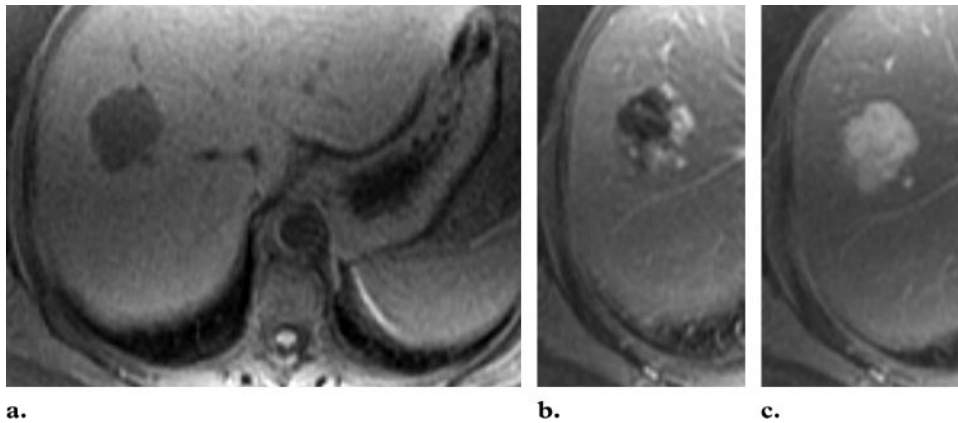
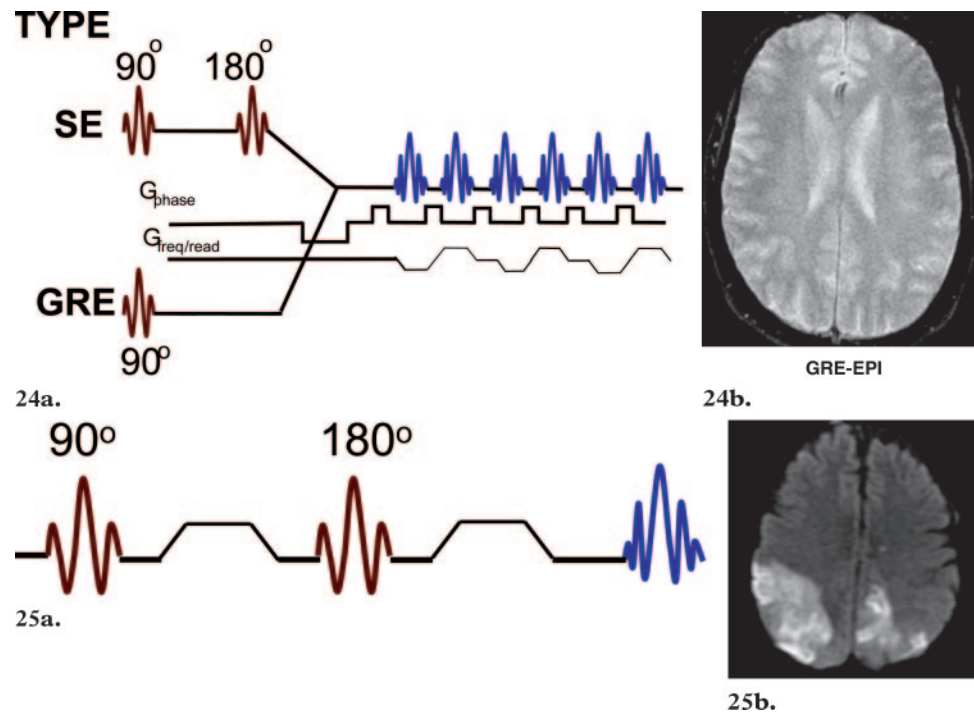


**Figure 23.** Spoiled GRE sequences for detection of liver hemangioma. **(a)** Axial T1-weighted spoiled GRE image obtained with fat saturation shows a low-signal-intensity lesion in the right lobe of the liver. **(b, c)** Axial multiphase T1-weighted spoiled GRE images obtained with gadolinium show nodular discontinuous peripheral enhancement immediately after intravenous contrast material injection and in the arterial phase **(b)**, with gradual filling over time in the venous phase **(c)**, features that help confirm the presence of a hemangioma.

**Fully Refocused GRE.**—The fundamental difference between partially refocused and fully refocused GRE sequences is that all the gradients in the latter are refocused. In addition, the phase of the RF pulse is alternated between  $0^\circ$  and  $180^\circ$  with each successive pulse in the sequence, and this alternation results in signal improvement. Steady-state free precession (SSFP), a technique in which a pulse is repeatedly applied with short TRs, also may be used in this type of GRE sequence (21). The tissue contrast produced with SSFP sequences is more complicated because it depends on  $T_2/T_1$ , with the signal generated being proportional to the square root of  $T_2/T_1$  (Fig 22b). Because images acquired with fully refocused GRE sequences are very susceptible to artifacts caused by magnetic field inhomogeneities, subsequent TRs must be very short (typically,  $<5$  msec). SSFP sequences are typically fast, provide

a high signal-to-noise ratio, and are very useful for cardiac imaging (Fig 22b), interventional MR imaging, and high-resolution imaging of the internal auditory canal.

**Spoiled GRE.**—Any remaining  $T_2^*$  effects created by the steady state may affect tissue contrast, making the GRE sequence more similar to T2 weighting, or may lead to streaking artifact. Therefore, in incoherent or spoiled GRE sequences, a spoiler RF pulse or gradient is used to eradicate any remaining transverse magnetization after each echo, thereby producing the same effect as T1 or proton-density weighting (Fig 22c) (19). Spoiled GRE sequences are especially useful for contrast material-enhanced MR imaging (Fig 23) and cardiac imaging.



**Figures 24, 25.** (24a) Echo-planar imaging sequence diagram. (24b) Axial T2-weighted echo-planar image (EPI) of the brain, obtained with the pulse sequence shown in 24a. (25a) Diffusion-weighted imaging sequence diagram. (25b) Axial diffusion-weighted brain image shows areas of restricted diffusion with high signal intensity.

### Echo-planar Imaging

With echo-planar imaging, a single echo train is used to collect data from all lines of k-space during one TR. Use of this technique shortens the acquisition time substantially (22). There are two types of echo-planar imaging sequences: SE and GRE sequences (Fig 24). All the lines of k-space can be acquired in a single TR (in single-shot echo-planar imaging) or in two or more TRs (in multishot echo-planar imaging). The phase-encoding gradient and the frequency-encoding (or readout) gradient are turned on and off very rapidly, a technique that allows the rapid filling of k-space. In this sense, echo-planar imaging can be considered a multiecho variant of the GRE sequence, in the same way that fast SE is a multiecho variant of the SE sequence. Echo-planar imaging is now a technique of choice for diffusion-weighted imaging, for which an echo-planar SE sequence typically is used (Fig 25). Echo-planar imaging is more vulnerable to magnetic susceptibility effects and provides greater tissue contrast than does imaging with standard GRE sequences; therefore, echo-planar imaging sequences are widely used to assess cerebral perfusion.

### Diffusion-weighted Imaging

Diffusion weighting enables one to distinguish between rapid diffusion of protons (unrestricted diffusion) and slow diffusion of protons (restricted diffusion) (23). For diffusion-weighted imaging, either an echo-planar or a fast GRE sequence is used (Fig 25), and two equal gradient pulses are applied (one on each side of the 180° RF pulse in echo-planar sequences). If no net movement of spinning nuclei occurs between the applications of the gradient pulses, the first gradient dephases the spins and the second rephases them; therefore, high signal intensity is seen. If there is net movement, the protons are not affected by both gradients (they may undergo dephasing but not rephasing, or vice versa); therefore, the signal intensity is decreased (Figs 25, 26).

One of the major uses for diffusion-weighted imaging sequences is in the diagnosis of recent stroke. However, diffusion-weighted sequences are usually applied in conjunction with apparent diffusion coefficient (ADC) mapping techniques (Fig 27). For the calculation of ADC maps, two sets of images are required: one set obtained without application of a diffusion gradient (which have an appearance similar to that of T2-weighted

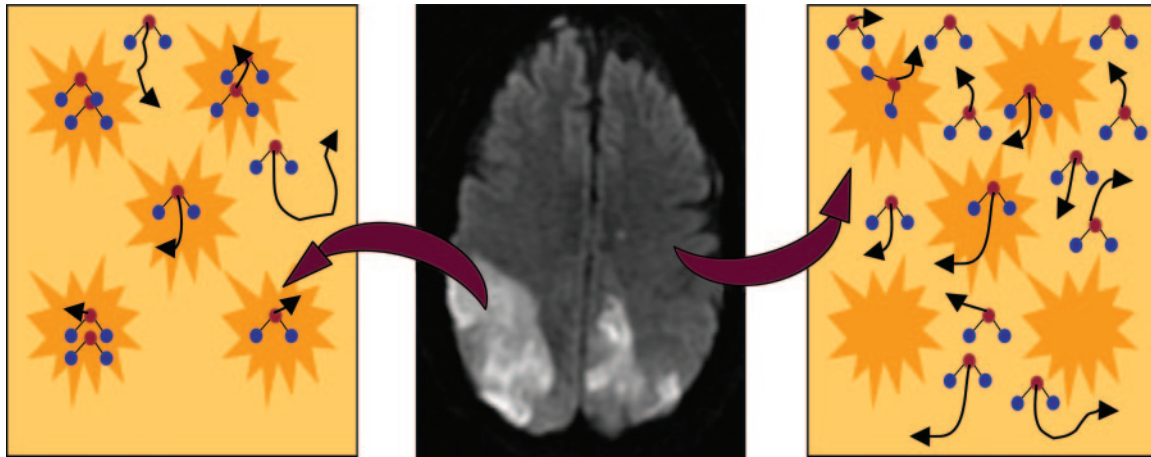


**Figure 26.** Schematics and corresponding diffusion-weighted brain image show areas of restricted (left) and unrestricted (right) diffusion.

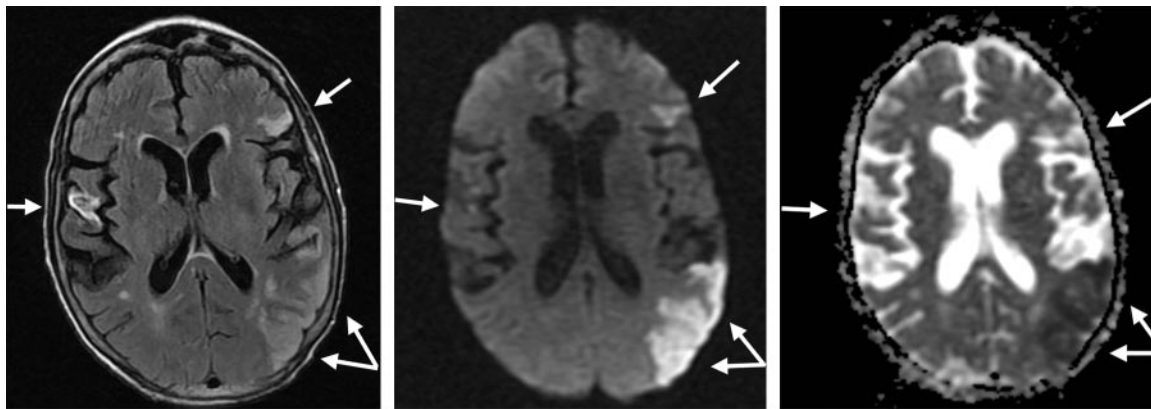


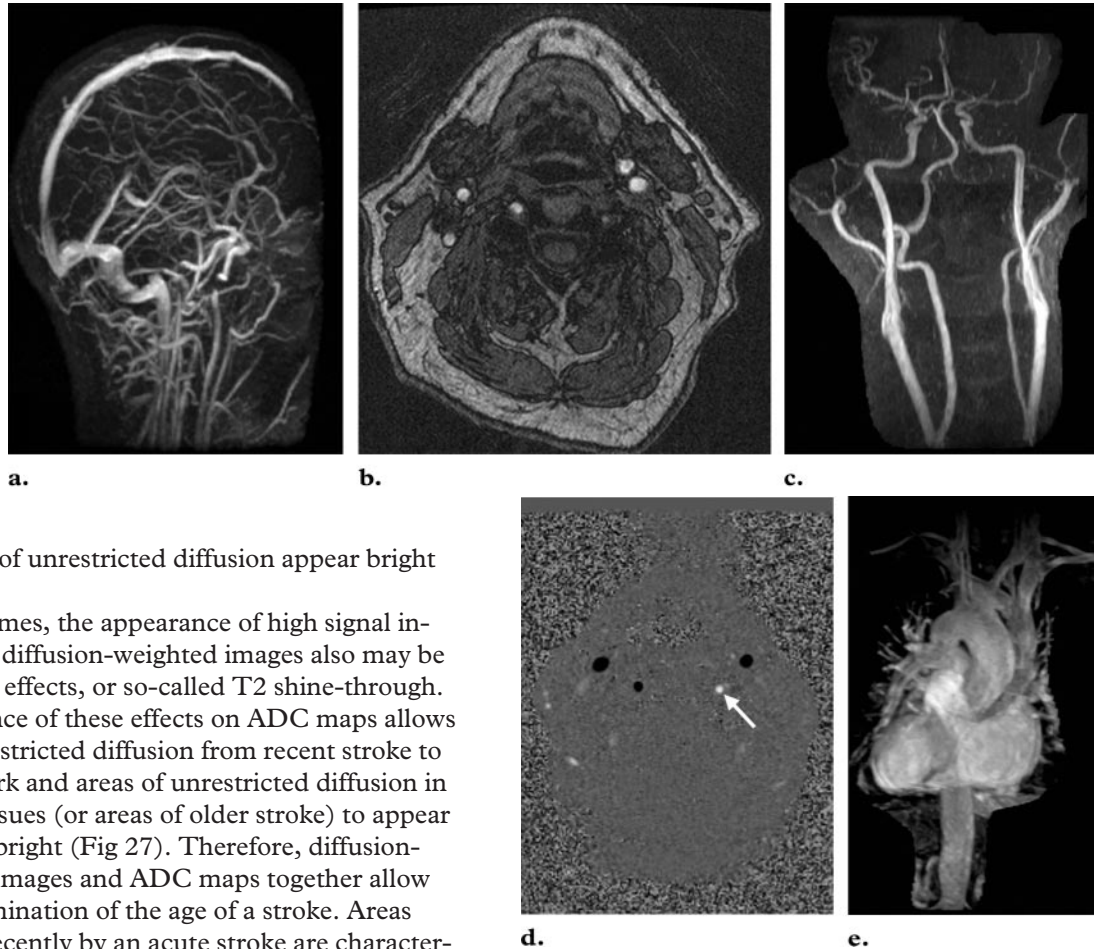
**Figure 27.** Combination of FLAIR and diffusion-weighted imaging with ADC mapping for depiction of effects of multiple strokes. **(a)** Axial T2-weighted FLAIR image shows three areas affected by strokes (arrows). **(b, c)** Axial diffusion-weighted echo-planar image **(b)** and ADC map **(c)** allow determination of the age of the strokes: The affected areas of the right frontal operculum and left frontal lobe (single arrows) show no evidence of restricted diffusion; this finding indicates that the stroke is old. In contrast, the affected area of the left parietal lobe (double arrows) appears bright in **b** and dark in **c**, evidence of restricted diffusion indicative of the most recent stroke. The area of the second most recent stroke, that in the left frontal lobe (single arrow), appears bright in both **b** and **c**; and the area of the oldest stroke, that in the right frontal operculum (single arrow), appears dark in **b** and bright in **c**.

images), and one obtained with a diffusion gradient. The ADC calculation is based on the negative logarithm of the ratio of those two image sets (images obtained with diffusion weighting compared with those obtained without diffusion weighting).

For example, let us assume that we have a region of restricted diffusion caused by an acute stroke. In the set of images obtained without a diffusion gradient, the restricted diffusion has an arbitrary signal intensity value of 10. In the set of images obtained with the diffusion gradient, it has an arbitrary signal intensity value of 5 (ie, some, but not profound, signal loss). The ratio of the

two has a value of 0.5 (the negative logarithm of 0.5 is 0.7). Now let us assume that we have a region of normal brain tissue with unrestricted diffusion. On images obtained without a diffusion gradient, the normal brain has an arbitrary signal intensity of 10. On images obtained with the diffusion gradient, it has an arbitrary signal intensity of 2. The ratio of the two has a value of 0.2 (the negative logarithm of 0.2 is 1.6). For this reason, areas of restricted diffusion appear dark on ADC maps (since the ADC values are scaled to the negative logarithm of the signal intensity ratio),

**Figure 28.** Comparison of MR angiographic images obtained with different sequences. (a) Maximum intensity projection from 2D time-of-flight imaging of the cerebral veins. (b) Axial image obtained with MOTSA. (c) Maximum intensity projection from MOTSA data (same examination as b). (d) Phase-contrast image shows left subclavian steal syndrome. In this example, caudal-to-cranial flow appears dark, and cranial-to-caudal flow appears bright. The left vertebral artery appears bright (arrow), a feature that indicates subclavian steal. (e) Maximum intensity projection from contrast-enhanced MR angiography at the level of the heart, aorta, and vessels of the aortic arch.



and areas of unrestricted diffusion appear bright (Fig 27).

Sometimes, the appearance of high signal intensity on diffusion-weighted images also may be due to T2 effects, or so-called T2 shine-through. The absence of these effects on ADC maps allows areas of restricted diffusion from recent stroke to appear dark and areas of unrestricted diffusion in remote tissues (or areas of older stroke) to appear relatively bright (Fig 27). Therefore, diffusion-weighted images and ADC maps together allow the determination of the age of a stroke. Areas affected recently by an acute stroke are characterized by restricted diffusion (depicted as bright areas on diffusion-weighted images and as dark areas on ADC maps); those affected recently by a subacute stroke appear somewhat bright on diffusion-weighted images and may appear moderately bright on ADC maps. Areas affected by old strokes are depicted as dark areas on diffusion-weighted images and bright areas on ADC maps.

### MR Angiography

The most common MR angiographic techniques are time-of-flight imaging, multiple overlapping thin-slab acquisitions (MOTSA), phase-contrast imaging, and contrast-enhanced MR angiography.

**Time-of-Flight Imaging and MOTSA.**—In these sequences, multiple RF pulses applied with short TRs saturate the spins in stationary tissues (24,25). This results in suppression of the signal from stationary tissues in the imaging slab. In-flowing blood is unaffected by the repetitive RF pulses; therefore, as it enters the imaging slab, its signal is not suppressed and appears hyperintense compared with that of stationary tissue. Time-of-flight imaging may be 2D, with section-by-section acquisition (Fig 28a), or 3D, with acquisition of a larger volume. MOTSA is the hybrid result of 2D and 3D time-of-flight imaging. Each slab in MOTSA is thinner than the typical slab in a single 3D time-of-flight image acquisition and,

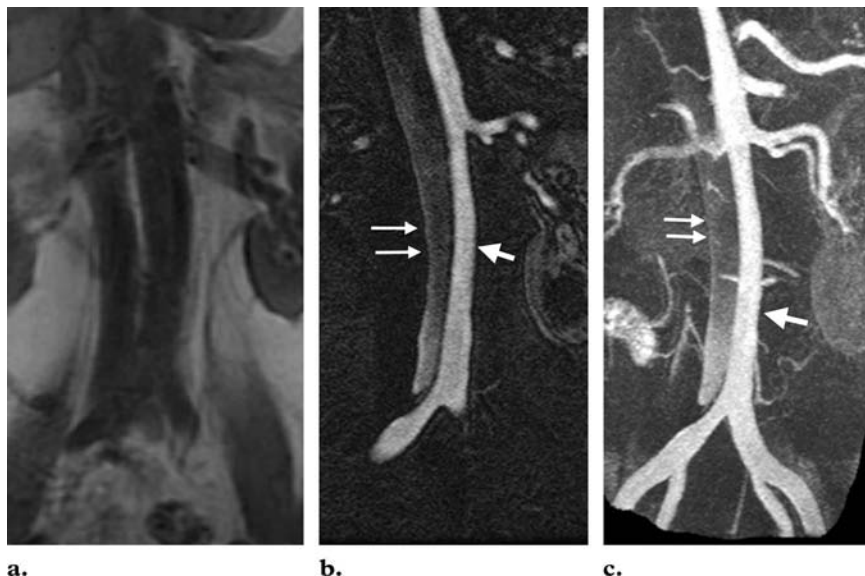


**Figure 29.** Comparison of GRE and contrast-enhanced MR angiographic sequences for depiction of type B aortic dissection. (a) Coronal T1-weighted spoiled GRE image does not clearly depict aortic dissection. (b, c) Coronal contrast-enhanced MR angiogram (b) and maximum intensity projection (c) obtained with a gadolinium-based contrast agent elegantly demonstrate the true lumen (single arrow) and false lumen (double arrows).

thus, is less deleteriously affected by distal saturation (Fig 28b, 28c). Images can be reviewed as individual sections or as maximum intensity projections. To obtain the latter, the maximal signal intensity is selected from stacks of images to produce 3D maps (Fig 28b, 28c).

**Phase-Contrast Imaging.**—Phase-contrast imaging provides information about the phase (or direction) of flow and the velocity (or magnitude) of flow (26). It requires two measurements that are sensitized to flow in different directions; typically, one measurement is sensitized to flow in one direction, and the second is sensitized equally to flow in the opposite direction. Both measurements are subtracted to eliminate any contribution to image phase that does not arise from flow or motion. As a result, no signal is detected from stationary tissue; signal is received only from flowing blood. Subtraction of the phase data yields spatial measures of flow velocity. Phase-contrast images also can be reconstructed as angiograms on the basis of the magnitude imaging data. Phase-contrast images can be either 2D or 3D.

Different conventions exist for the interpretation of signal seen on directional and velocity phase-contrast images. One convention is that high signal is seen from flow that moves from a superior location to an inferior one, from right to left, and from an anterior to a posterior location. No signal (a signal void) is seen from flow that

moves from an inferior to a superior location, from left to right, or from a posterior to an anterior location (Fig 28d).

**Contrast-enhanced MR Angiography.**—In contrast-enhanced MR angiography, an intravenous contrast material (usually gadopentetate dimeglumine or another gadolinium-based agent) is used (27). Such agents typically shorten the T1 of blood (ie, hasten the recovery of longitudinal magnetization), so a higher-magnitude net magnetization vector is available to be flipped with the next TR, a condition that results in high signal intensity on T1-weighted images (Fig 28e). Contrast-enhanced MR angiography also can be performed with 2D or 3D methods. A clinical example of the use of this modality can be seen in Figure 29.

### Fat-related Imaging Techniques

**Fat Signal Suppression.**—Fat has high signal intensity on T1-weighted images because of its short T1. However, it is desirable sometimes (eg, at contrast-enhanced MR imaging) to null the signal from fat so that the signal from other tissues is more conspicuous. For this purpose, fat saturation may be applied. There are various methods for achieving fat saturation.

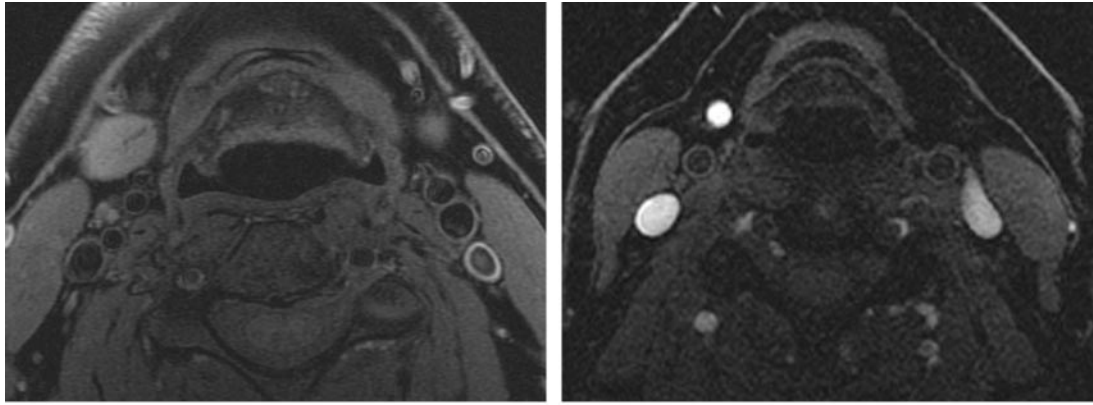
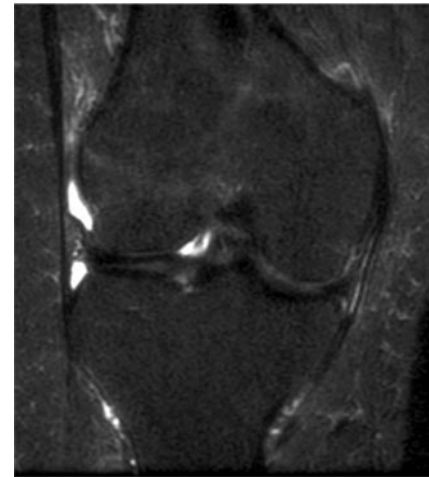


**Figure 30.** Comparison of fat-saturation and water-excitation sequences at MR imaging. **(a)** Axial T1-weighted image of the neck obtained with a double inversion-recovery pulse sequence with fat saturation. **(b)** Coronal STIR image of the knee. **(c)** Axial T1-weighted GRE image of the neck, obtained with a water-excitation sequence.

First, fat saturation may be obtained by applying an RF pulse at the beginning of any sequence and following it immediately with a spoiler or crusher gradient that shifts the net magnetization vector of fat so that it has no longitudinal magnetization at the start of the image acquisition (28). Subsequently, because no transverse magnetization for fat is generated, no signal from fat is seen. This is the method most commonly used for nulling the signal from fat (Fig 30a), and it is often used in contrast-enhanced MR imaging. As discussed previously, fat-saturation pulses are affected by magnetic field inhomogeneities (eg, between skin and air). Incomplete fat saturation is sometimes observed when such pulses are used (Fig 16), because of imperfect selective excitation of the resonance frequency of fat.

Fat-saturation techniques are useful clinically for the diagnosis of liposarcomas, in which the high signal intensity normally observed on T1-weighted images appears suppressed on images obtained with fat saturation, and of lipomas (Fig 31). The addition of a fat-saturation pulse to a fast SE sequence at musculoskeletal MR imaging can result in highly sensitive depiction of edema and highlight the extent of pathologic change in bone marrow.



**b.**

The second method for achieving fat saturation is the use of an inversion-recovery pulse to null the signal from fat (14). When the net magnetization vector of fat just passes the null point, little or no longitudinal magnetization is present in fat; thus, when the net magnetization vector for fat is flipped by the  $90^\circ$  RF pulse (Fig 13), the transverse magnetization of fat is insignificant. Therefore, no signal is generated from fat. One example of this type of sequence is STIR (Figs 13, 16, 30b).

The third method of fat saturation involves the application of a water-excitation technique so that only tissues containing water have transverse magnetization (and fat has no transverse magnetization) (29). Because no transverse magnetization is generated in fat, no signal is generated from fat. An example of a water-excitation technique is the spectral-spatial RF pulse (Fig 30c).

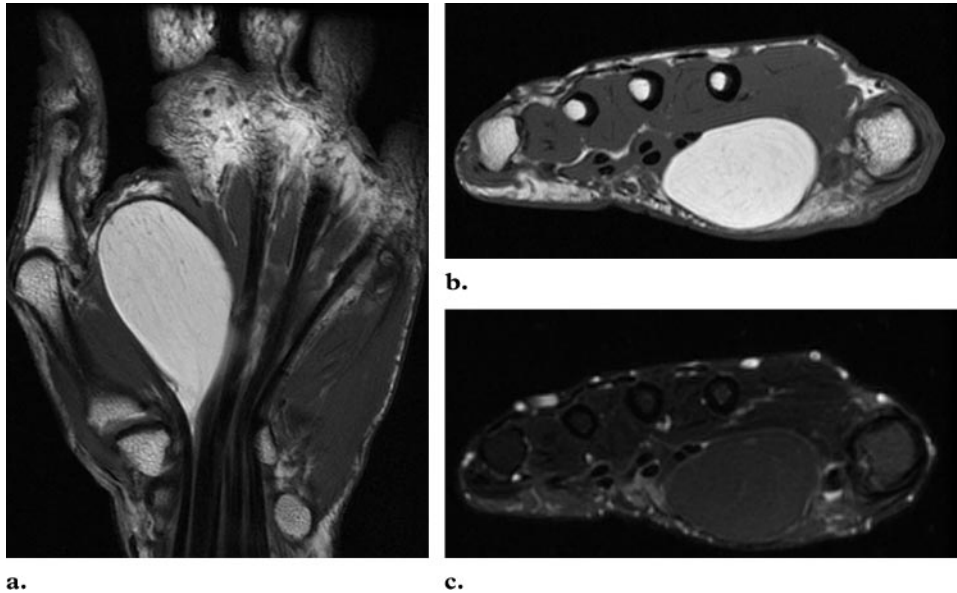


**Figure 31.** Use of fat suppression for detection of simple lipoma. (a, b) Coronal (a) and axial (b) T1-weighted SE images show a large ovoid lesion in the palm of the hand with signal intensity paralleling that of subcutaneous fat. (c) Axial T2-weighted fast SE image obtained with fat saturation shows uniform suppression of signal throughout the lesion, an indication that the lesion is composed entirely of fat.

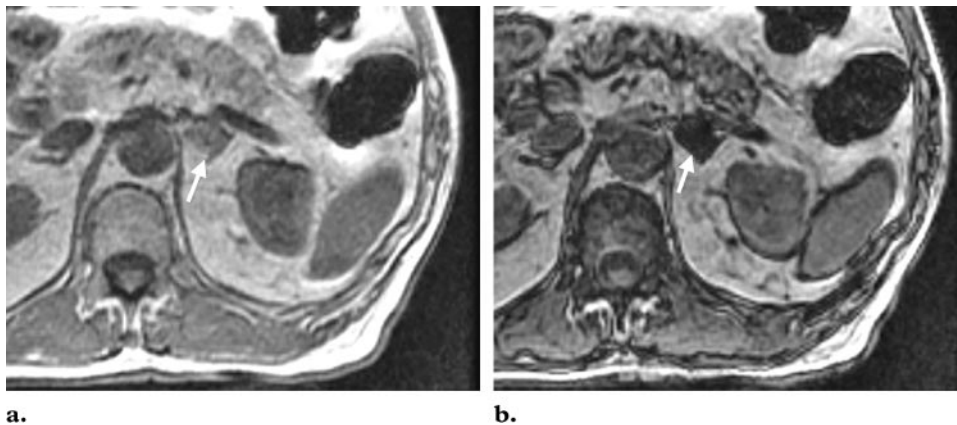


**Figure 32.** Comparison of axial T1-weighted spoiled GRE images obtained at 1.5 T with in-phase imaging (TE = 4.2 msec) (a) and with out-of-phase imaging (TE = 2.1 msec) (b) shows an adrenal adenoma (arrow), which appears in b as an area of signal void due to cancellation of the signal from microscopic fat.

**In-Phase and Out-of-Phase Imaging.**—In- and out-of-phase imaging is routinely used to depict microscopic fat, which is helpful for distinguishing adrenal adenomas from adrenal carcinomas. Because of the different chemical environments of  $^1\text{H}$  in fat ( $\text{CH}_2$ ) and water ( $\text{H}_2\text{O}$ ),  $^1\text{H}$  nuclei precess at different rates. With this sequence, usually a spoiled GRE, fat and water are

imaged when their  $^1\text{H}$  nuclei are spinning in phase with each other (TE = 4.2 msec at 1.5 T) and out of phase with each other (TE = 2.1 msec at 1.5 T). If microscopic fat is present, its signal is nulled (canceled out) on the out-of-phase images (Fig 32) (30).

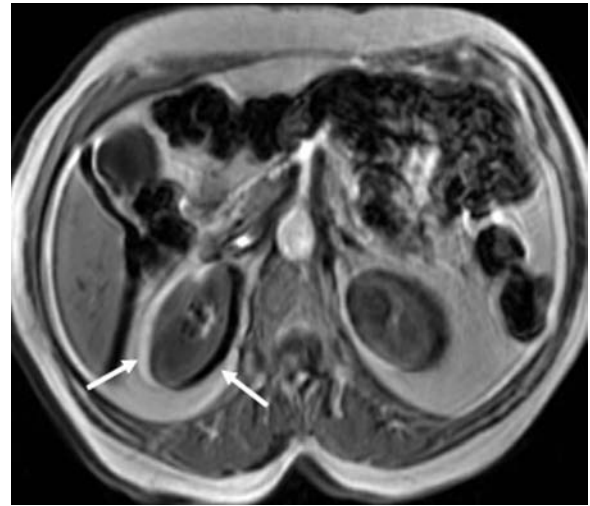
**Teaching  
Point**

**Chemical Shift Artifact.**—Chemical shift is an artifact from fat that deserves special mention. This artifact occurs only in the frequency-encoding (readout) direction because of differences between the chemical environments surrounding the  $^1\text{H}$  atoms in water and fat. Fat and water precess at different frequencies, a condition that results in misregistration due to a chemical shift effect on the encoding of signal from the protons in fat and water. The result is the appearance of a dark rim at one edge of an object (eg, a kidney) and a bright rim at the opposite edge (Fig 33) (1–3).

### Specific Absorption Rate

MR imaging is usually thought of as a safe imaging modality because no ionizing radiation is used to obtain the images. However, it is important that radiologists who work in MR imaging be acquainted with the concept of the specific absorption rate (SAR) (31). As you may remember, the RF pulse that is used to flip the net magnetization vector into the transverse plane is an energy pulse. The energy from the RF pulse is deposited in the patient. The SAR is a measure of the rate at which that RF energy (measured in watts) is dissipated in tissue, per unit of tissue mass (measured in kilograms).

The SAR is proportional to  $B_0^2\alpha^2D$ , where  $B_0$  is the field strength,  $\alpha$  is the flip angle, and  $D$  is the duty cycle (or TR). By implication, if the field strength used to image the patient is doubled (eg, from 1.5 to 3.0 T), the SAR increases fourfold. Likewise, if the flip angle is doubled (eg, from  $15^\circ$  to  $30^\circ$ ), the SAR increases fourfold. Therefore, SE sequences and SE-based (particularly inversion-recovery) sequences in which flip angles of  $90^\circ$  and  $180^\circ$  are used are associated with a higher

**Teaching  
Point**


**Figure 33.** Chemical shift artifact at water-fat interfaces. Axial T1-weighted GRE image at the level of the kidneys shows a dark rim at one edge of the kidney and a bright rim at the opposite edge (arrows), an artifact that results from differences in the precessional frequencies of fat and water.

SAR than are GRE sequences, which do not always require a  $90^\circ$  flip angle. Similarly, if the duty cycle is doubled (if TR is decreased by one-half), the SAR also is doubled.

### Summary

The use of MR imaging likely will continue to increase exponentially in the near term; therefore, an understanding of the physical underpinnings of the modality is of paramount importance. In this article, we describe the physical basis of the MR pulse sequences most commonly used in routine clinical imaging and review the specific advantages of particular contrast weighting techniques and pulse sequences for the visualization of various tissues. We hope this information will provide a foundation for a fuller understanding of MR imaging and all that it has to offer.

## References

1. Westbrook C, Kaut C. MRI in practice. 2nd ed. Oxford, England: Blackwell Science, 1998.
2. Brown MA, Semelka RC. MR imaging abbreviations, definitions, and descriptions: a review. *Radiology* 1999;213:647-662.
3. Westbrook C. MRI at a glance. Oxford, England: Blackwell Science, 2002.
4. Brant WE. Diagnostic imaging methods. In: Brant WE, Helms CA, eds. *Fundamentals of diagnostic radiology*. 2nd ed. Philadelphia, Pa: Lippincott Williams & Wilkins, 1999; 9-21.
5. Bloch F. Nuclear induction. *Phys Rev* 1946;70:460-474.
6. Purcell EM, Torrey HC, Pound RV. Resonance absorption by nuclear magnetic moments in a solid. *Phys Rev* 1946;69:37-38.
7. Bloembergen N, Purcell EM, Pound RV. Relaxation effects in nuclear magnetic resonance absorption. *Phys Rev* 1948;73:679-712.
8. Hoult DI, Richards RE. The signal-to-noise ratio of the nuclear magnetic resonance experiment. *J Magn Reson* 1976;24:71-85.
9. Damadian R. Tumor detection by nuclear magnetic resonance. *Science* 1971;171:1151-1153.
10. Hahn EL. Spin echoes. *Phys Rev* 1950;80:580-594.
11. Kumar A, Welti D, Ernst RR. NMR Fourier zeugmatography. *J Magn Reson* 1975;18:69-83.
12. Twieg DB. The k-trajectory formulation of the NMR imaging process with applications in analysis and synthesis of imaging methods. *Med Phys* 1983;10:610-621.
13. Meiboom S, Gill D. Modified spin-echo method for measuring nuclear relaxation times. *Rev Sci Instrum* 1958;29:688-691.
14. Fleckenstein JL, Archer BT, Barker BA, Vaughan JT, Parkey RW, Peshock RM. Fast short-tau inversion-recovery MR imaging. *Radiology* 1991;179:499-504.
15. De Coene B, Hajnal JV, Gatehouse P, et al. MR of the brain using fluid-attenuated inversion recovery (FLAIR) pulse sequences. *AJNR Am J Neuroradiol* 1992;13:1555-1564.
16. Frahm J, Haase A, Matthaei D. Rapid three-dimensional MR imaging using the FLASH technique. *J Comput Assist Tomogr* 1986;10:363-368.
17. Wendt RE 3rd, Wilcott MR 3rd, Nitz W, Murphy PH, Bryan RN. MR imaging of susceptibility-induced magnetic field inhomogeneities. *Radiology* 1988;168:837-841.
18. Kucharczyk J, Asgari H, Mintorovitch J, et al. Magnetic resonance imaging of brain perfusion using the nonionic contrast agents Dy-DTPA-BMA and Gd-DTPA-BMA. *Invest Radiol* 1991;26(suppl 1):S250-S252.
19. Crawley AP, Wood ML, Henkelman RM. Elimination of transverse coherences in FLASH MRI. *Magn Reson Med* 1988;8:248-260.
20. Hawkes RC, Patz S. Rapid Fourier imaging using steady-state free precession. *Magn Reson Med* 1987;4:9-23.
21. Evans AJ, Hedlund LW, Herfkens RJ, Utz JA, Fram EK, Blinder RA. Evaluation of steady and pulsatile flow with dynamic MRI using limited flip angles and gradient refocused echoes. *Magn Reson Imaging* 1987;5:475-482.
22. Mansfield P. Multiplanar image formation using NMR spin echoes. *J Phys C Solid State Phys* 1977;10(3):L55-L58.
23. Stejskal EO, Tanner JE. Spin diffusion measurements: spin-echoes in the presence of a time-dependent field gradient. *J Chem Phys* 1965;42:288-292.
24. Bradley WG Jr, Waluch V, Lai KS, Fernandez EJ, Spalter C. The appearance of rapidly flowing blood on magnetic resonance images. *AJR Am J Roentgenol* 1984;143:1167-1174.
25. Nishimura DG. Time-of-flight angiography. *Magn Reson Med* 1990;14:194-201.
26. Dumoulin CL, Hart HR Jr. Magnetic resonance angiography. *Radiology* 1986;161:717-720.
27. Creasy JL, Price RR, Presbrey T, Goins D, Partain CL, Kessler RM. Gadolinium-enhanced MR angiography. *Radiology* 1990;175:280-283.
28. Haase A, Frahm J, Hanicke W, Matthaei D. 1H NMR chemical shift selective (CHESS) imaging. *Phys Med Biol* 1985;30:341-344.
29. Meyer CH, Pauly JM, Macovski A, Nishimura DG. Simultaneous spatial and spectral selective excitation. *Magn Reson Med* 1990;15:287-304.
30. Dixon WT. Simple proton spectroscopic imaging. *Radiology* 1984;153:189-194.
31. Adair ER, Berglund LG. On the thermoregulatory consequences of NMR imaging. *Magn Reson Imaging* 1986;4:321-333.

## Teaching Points for MR Pulse Sequences: What Every Radiologist Wants to Know but Is Afraid to Ask

*Richard Bitar, MD, MSc et al*

RadioGraphics 2006; 26:513–537 • Published online 10.1148/rg.262055063 • Content Codes: MR PH

---

### Page 515

The transverse component of the net magnetization vector induces a current in the receiver coil. For the induction of current, the nuclei must be spinning in phase; as the nuclei gradually spin out of phase, the signal induced in the coil decreases.

### Page 519

There are only two fundamental types of MR pulse sequences: SE and GRE. All other MR sequences are variations of these, with different parameters added on.

### Page 526

Because gradients do not refocus field inhomogeneities, GRE sequences with long TEs are T2\* weighted (because of magnetic susceptibility) rather than T2 weighted like SE sequences.

### Page 536

Chemical shift is an artifact from fat that deserves special mention. This artifact occurs only in the frequency-encoding (readout) direction because of differences between the chemical environments surrounding the <sup>1</sup>H atoms in water and fat. Fat and water precess at different frequencies, a condition that results in misregistration due to a chemical shift effect on the encoding of signal from the protons in fat and water. The result is the appearance of a dark rim at one edge of an object (eg, a kidney) and a bright rim at the opposite edge (1–3).

### Page 536

It is important that radiologists who work in MR imaging be acquainted with the concept of the specific absorption rate (SAR) (31). As you may remember, the RF pulse that is used to flip the net magnetization vector into the transverse plane is an energy pulse. The energy from the RF pulse is deposited in the patient. The SAR is a measure of the rate at which that RF energy (measured in watts) is dissipated in tissue, per unit of tissue mass (measured in kilograms).